Bulletin of Earthquake Engineering
https://doi.org/10.1007/s10518-021-01156-3

ORIGINAL ARTICLE

Cyclic engagement of hysteretic steel dampers in braced buildings: a parametric investigation

Emanuele Gandelli[1] · **Dario De Domenico**[2] · **Virginio Quaglini**[1]

Received: 31 January 2021 / Accepted: 28 May 2021
© The Author(s) 2021

Abstract
Hysteretic steel dampers have been effectively used to improve the seismic performance of framed buildings by confining the dissipation of seismic energy into sacrifical, replaceable devices which are not part of the gravity framing system. The number of cycles sustained by the dampers during the earthquake is a primary design parameter, since it can be associated to low-cycle fatigue, with ensuing degradation of the mechanical properties and potential failure of the system. Current standards, like e.g. the European code EN 15129, indeed prescribe, for the initial qualification and the production control of hysteretic steel dampers, cyclic tests in which the devices are assessed over ten cycles with amplitude equal to the seismic design displacement d_{bd}. This paper presents a parametric study focused on the number of effective cycles of the damper during a design earthquake in order to assess the reliability of the testing procedure proposed by the standards. The study considers typical applications of hysteretic steel dampers in low and medium-rise steel and reinforced concrete framed buildings and different ductility requirements. The results point out that the cyclic engagement of the damper is primarily affected by the fundamental period of the braced building and the design spectrum, and that, depending on these parameters, the actual number of cycles can be substantially smaller or larger that recommended by the standards. A more refined criterion for establishing the number of cycles to be implemented in testing protocols is eventually formulated.

Keywords Supplemental energy dissipation · Braced frames · Code requirements · Parametric study · Number of effective cycles · Hysteretic steel dampers

✉ Emanuele Gandelli
emanuele.gandelli@polimi.it

[1] Department of Architecture, Built Environment and Construction Engineering, Politecnico Di Milano, Piazza Leonardo da Vinci 31, 20133 Milano, Italy

[2] Department of Engineering, University of Messina, Contrada Di Dio, Sant'Agata, 98166 Messina, Italy

Published online: 01 July 2021

1 Introduction

During major earthquakes civil constructions are subjected to large energy inputs, which can cause permanent structural damage and loss of life. To minimize casualties and economic losses, a structure needs to remain largely damage free. A viable design approach to improve the seismic performance of a structure consists in concentrating the dissipation of most of the earthquake input energy in sacrificial elements that are not part of the gravity framing system (Christopolous and Filiatrault 2006). This philosophy allows to minimize damage in structural and non-structural elements, increase life-safety and achieve a desired level of performance (Di Cesare et al. 2014; 2017a). Moreover, after an earthquake, these sacrificial elements can be repaired or replaced, reducing cost and interruption of human occupancy and operation, with evident economic and social benefits (Di Cesare et al. 2020). The concept of using supplemental systems to increase the damping in a structure was proposed in the late 1960s (Muto et al. 1969; Kelly et al. 1972; Skinner et al. 1974) and nowadays supplemental energy dissipation or damping systems are one of the most popular and cost-effective approaches to mitigate the seismic risk for both new and existing structures (De Domenico et al. 2020).

Energy dissipation devices can be classified in two main categories, namely Velocity Dependent Devices (VDDs) and Displacement Dependent Devices (DDDs) (Christopolous and Filiatrault 2006). The first category includes fluid dampers, where the dissipation is achieved through the lamination of a viscous fluid which is forced by a piston to flow through a valving system. The behavior of these devices strictly depends on the fluid velocity. Viscous fluid dampers are very versatile and can be designed to allow unconstrained slow thermal motions as well as to provide controlled damping of a structure to protect from wind or earthquakes (Del Gobbo et al. 2018; Karavasilis et al. 2016; De Domenico et al. 2019; De Domenico and Ricciardi 2019). They are typically employed in flexible structures subjected to large and rapid movements like bridges and tall buildings. The second category comprises hysteretic dampers and is further divided into steel dampers, friction dampers and metal extrusion dampers (Nabid et al. 2018), depending on the mechanism used to dissipate the seismic energy. The constitutive law of these devices is mainly dependent on the imposed displacement. Most of the dampers used in residential, school and industrial buildings belong indeed to this category. In these buildings, the dampers are typically inserted into braces which convert the interstorey drift into the axial deflection of the damper. The theoretical force—displacement curves of hysteretic dampers are shown in Fig. 1, where d_y is the yield displacement of the device, d_{max} is the maximum displacement in a cycle, and F_y and F_{max} are the axial force at d_y and d_{max}, respectively; the area included in the curve corresponds to the energy dissipated during a cycle. The ratio between the maximum displacement and the yield displacement defines the ductility factor μ_D of the damper.

Among hysteretic dampers, devices based on the plastic deformation of mild steel are the most popular due to their stability at high levels of deformation, negligible degradation and reliability during repeated cycles, and good resistance to weathering and aging. Different types of steel dampers have been proposed and tested for implementation in structures (Javanmardi et al. 2020; Di Cesare et al. 2014; 2017b; Pampanin et al. 2017; Morillas et al. 2020; Mohsenian et al. 2018), including torsional or flexural beams (Montuori et al. 2015), single-axis dampers (Skinner et al. 1974) U-strips (Baird et al. 2014; Buchanan et al. 2007), buckling-restrained braces (BRB) (Watanabe et al. 1988; Foti et al. 2020), crescent shaped braces (CSBs) (Palermo et al. 2014, 2015, 2017; Kammouh et al. 2018), and energy

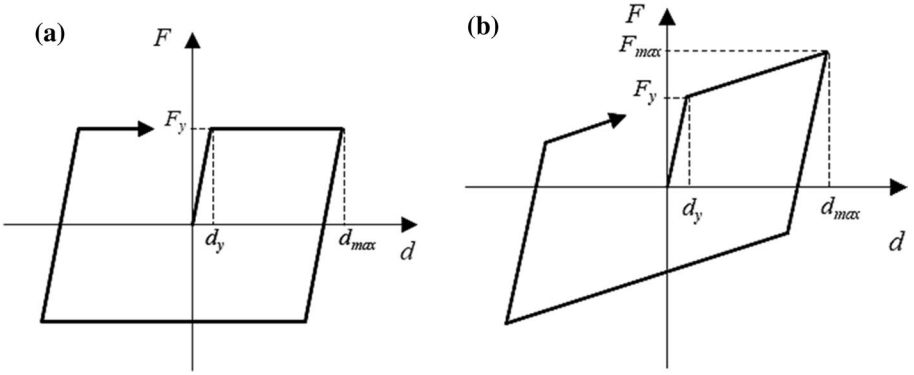

Fig. 1 Theoretical hysteresis loops of hysteretic dampers: **a** with elastic-ideally plastic behavior; **b** with hardening behavior

dissipative steel cushions (Ozkaynak et al. 2018; Gullu et al. 2019). In parallel to the development of the hardware, viable design procedures and configurations of dissipative bracing systems incorporating metallic dampers have been envisaged for the seismic retrofitting of existing r.c and steel buildings (Akcelyan et al. 2016; Barbagallo et al. 2017; Bergami et al. 2013; Di Cesare et al. 2017a; Durucan et al. 2010; Mazza et al. 2015a; 2015b; 2016a, b; 2019; Nuzzo et al. 2019; O'Reilly et al. 2016; Gandelli et al. 2019; Mohammadi et Al. 2019) and for new constructions with different materials (Quintana et al. 2020; Nuzzo et al. 2020; Granello et al. 2020; Ponzo et al. 2019).

The performance of a hysteretic damper is defined by: (1) the force–displacement constitutive law, which is an inherent characteristic of the device; (2) the number of cycles sustained during the earthquake, which depends on the duration of the ground motion and the fundamental frequency of the structural system where the damper is employed. The number of cycles defines the total amount of energy dissipated by the system for a given displacement but is also associated to the degradation and possible failure of the device due to low-cycle fatigue (Morillas et al. 2020).

Testing of hysteretic dampers to verify their conformity to performance requirements is regulated by standards, like e.g. the EN 15129 (CEN, 2009), which is compulsory in the European Economic Area. According to the European standards, the force–displacement cycle of the damper shall be evaluated by imposing series of cyclic deformations at increasing amplitudes, namely at 25, 50 and 100% of the design displacement d_{bd}. Five cycles for each intermediate amplitude and at least ten cycles for the maximum amplitude shall be applied. The conceptual diagram of the displacement histories is shown in Fig. 2, where d_{max} is the maximum displacement in the relevant cycles. If scaled specimens are used, test displacements and cycling frequency shall be consistently scaled. The device shall not break and shall keep its characteristics unchanged during test. Eventually, a ramp test shall be performed for the static evaluation of the failure displacement up to a displacement not less than the maximum displacement $\gamma_b \times \gamma_x \times d_{bd}$. The partial factor γ_b, not less than 1.1, is related to action effects other than seismic which can affect the initial configuration of the device. The reliability factor γ_x, equal or greater than 1, depends on the role that the devices play in the stability of the construction after the earthquake. When the damper is employed as a part of an isolation system, the reliability factor γ_x shall be taken as 1.2 for use in critical structures other than bridges (CEN 2004) and 1.5 for use in bridges (CEN 2005).

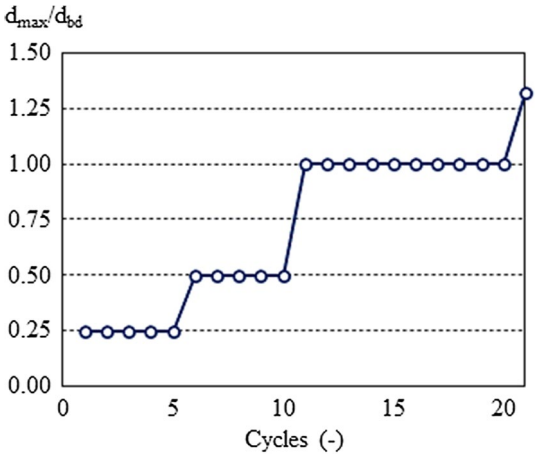

Fig. 2 Displacement history prescribed by EN 15,129 for qualification and factory production control tests

The specified test protocol shall be performed as Type Test, for the initial qualification of a device, and then repeated as factory production control test on a minimum of 2% of the devices of the supply, with a minimum of one device. The tested devices may be installed into the structure only if the fatigue resistance of their core elements is one order of magnitude greater than the number of cycles performed during the tests. In any other case, they shall not be installed into the structure, unless their mechanical characteristics are fully recovered, e.g., by replacing the nonlinear mechanism or the core elements.

To the authors' best knowledge, among the various parameters, the number of cycles to be imposed to the specimens deserves a careful investigation since it is not based on specific studies documented in literature. Moreover, the standard specifies that the number of ten cycles at $\pm d_{bd}$ is related to the use of dampers in seismic isolation systems producing fundamental periods of the order of 2 s, but if the fundamental period of the structural system in which the device is used is considerably less than 2 s, a "corresponding increase of the number of test cycles at $\pm d_{bd}$" shall be prescribed by the Structural Engineer; however a rationale specifying the correlation between the structural frequency and the number of cycle is missing.

The present study investigates, through a parametric study, the engagement of hysteretic dampers installed in bracing systems of framed buildings in terms of number of "effective cycles" accommodated during the design earthquake, in order to evaluate the suitability of the testing protocol recommended by the European standard. It is indeed of fundamental importance, for both manufacturers and work directors, to have at hand validated testing protocols which allow to assess the seismic performance of structural devices under benchmark conditions replicating the actual conditions the devices in practical applications. Moreover, a revision of the standard EN 15129 is in progress within the Technical Committee 340 of the European Standardization Center (CEN), and the improvement of the theoretical background is expected to enhance the technical level of the code.

The paper is organized as follows. The first Section presents the code requirements and justifies the motivations and aims of the work. Section 2 introduces the parametric investigation, which considers six buildings, representative of low and medium-rise structures made of either steel or reinforced concrete, six dampers' layouts accounting

for different ductility factors of the device (μ_D) or the frame (μ_F), and four seismic scenarios. In Sect. 3 the accuracy of non-linear time history (NLTH) analyses carried out using equivalent single degree of freedom (SDOF) equivalent instead of multi degree of freedom (MDOF) models of the damped building is evaluated; the use of SDOF model allows indeed a substantial reduction of computational time and data processing. In Sect. 4 the results of the parametric study are illustrated and discussed. The cyclic engagement of hysteretic dampers during an earthquake is demonstrated to depend on the fundamental period of the structure where the dampers are placed and the spectral characteristics of the ground motion. The code provisions are eventually checked against the numerical results of this parametric study, and improvements are suggested. Finally, Sect. 5 summarizes the main outcomes of the research.

2 Parametric investigation

A parametric investigation has been carried out in order to assess the number of "effective cycles" (defined in Sect. 3) sustained by DDD units installed in braced buildings. The parameters addressed in the study regard:

- The structural frame: six frames, representative of low and medium-rise structures made of either steel or reinforced concrete, have been considered (see Sect. 2.1);
- The seismic scenario: four response spectra have been defined by combining two seismic intensity levels, corresponding to either Ultimate Limit State (ULS) or Serviceability Limit State (SLS), and two soil categories, stiff (type A) or moderate-soft (type C). For each design spectrum, a set of fourteen ground motion records has been selected (see Sect. 2.2);
- The ductility factor of the hysteretic dampers;
- The target ductility of the braced frame at ULS (see Sect. 2.3).

For each layout of the braced frame, two equivalent SDOF formulations will be introduced in the next Sections. The first one employs linear equivalent response spectrum analyses and is aimed at defining the DDDs' mechanical properties (resulting in seventy-two different layouts—see Tables 7, 8 of the Appendix). The second equivalent SDOF formulation, where for sake of simplicity, both the bare frame and the DDD are modelled by means of elastic–plastic elements arranged in parallel, is later implemented in NLTH analyses in order to quantify the number of effective cycles of the DDD. A total of 2016 simulations (1008 at ULS plus 1008 at SLS) has been carried out. In future developments of this investigation the possible, although usually small ($k_{pl,D}/k_{el,D} < 0.1$, Di Cesare et al. 2017a), post-yielding hardening of steel hysteretic dampers will be also accounted for.

2.1 Case-study frames

Six case-study structures, including three steel frames and three reinforced concrete (RC) frames, have been examined, in order to envelope a wide range of fundamental periods of interest for conventional buildings. The steel frames are 2-, 4- and 8-storey moment resisting frames, with material and geometrical properties as specified in the INNOSEIS project (Vayas et al. 2017). The frames were designed in compliance with Eurocode 3 (EC3) (CEN

2003) and Eurocode 8 (EC8) (CEN 2004) considering gravity loads and low earthquake-induced loads, corresponding to a design spectrum for soil A and peak ground acceleration (PGA) equal to 0.2 g (g denoting the gravity acceleration). Sketches of the frames, with the main dimensions in plan and in elevation, and the steel profiles adopted in the design, are reported in Fig. 3. The RC frames correspond to three residential RC buildings (Faleschini et al. 2019). The frames, comprising 3-, 6- and 9-storey buildings, were designed according to the Italian Building Code (CSLLPP 2018) for a low seismicity zone (475-yr return

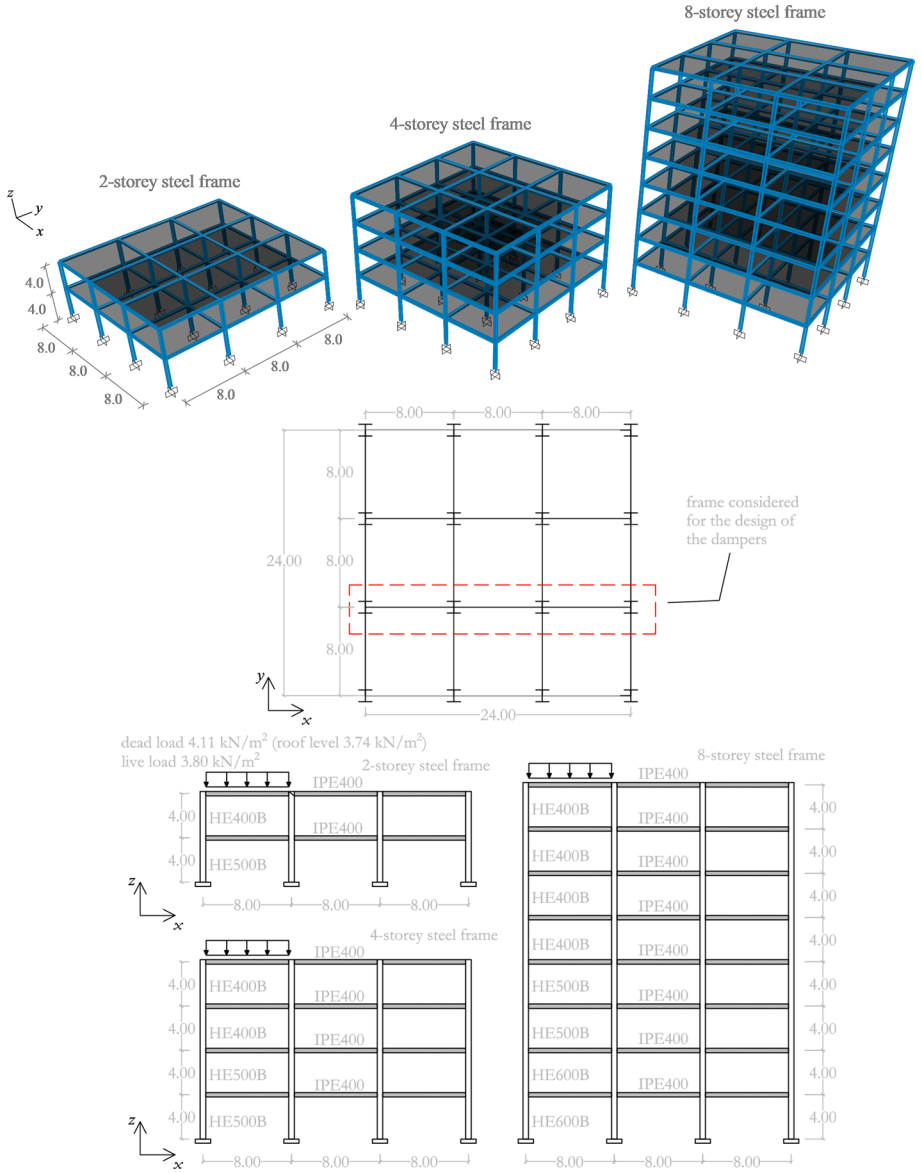

Fig. 3 Steel frames case-studies

period PGA = 0.195 g, soil type B) corresponding to the municipality of Pordenone, Italy. An overview of the RC frames with the main dimensions is given in Fig. 4, and the reinforcement details of each section are listed in Table 1.

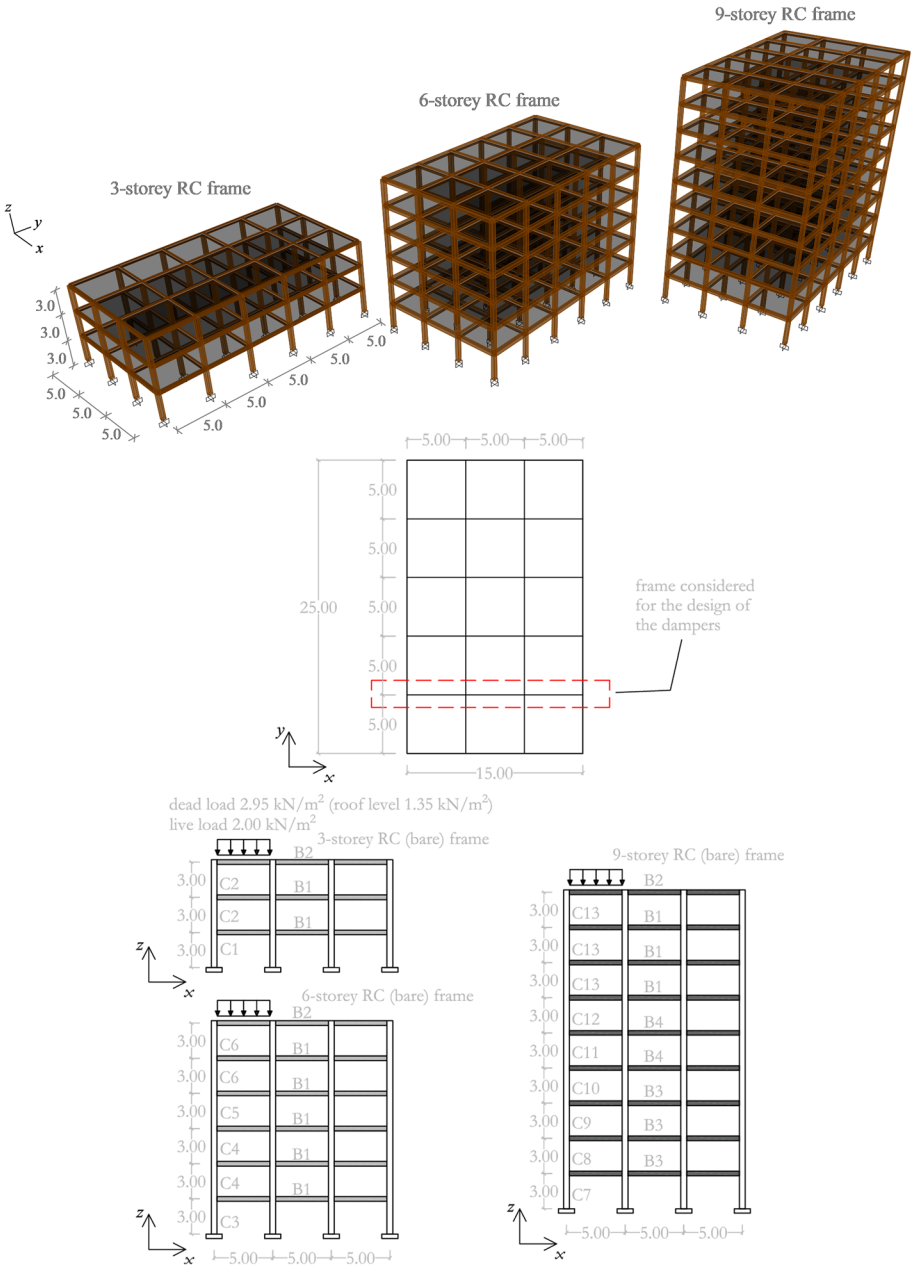

Fig. 4 RC frames case-studies

Table 1 Cross-section details of beams and columns of the RC frames (see Fig. 3)

ID	Section dimensions (cm)	Longitudinal reinforcement (top + bottom bars)	Transverse reinforcement (stirrups dimension/spacing at beam-column joint)
B1	30×40	$4 + 2\phi 16$	$\phi 8/8cm$
B2	30×40	$3 + 2\phi 16$	$\phi 8/8cm$
B3	40×50	$4 + 4\phi 16$	$\phi 8/10cm$
B4	30×50	$4 + 3\phi 16$	$\phi 8/10cm$
C1	40×40	$8\phi 18$	$\phi 10/8cm$
C2	40×40	$8\phi 18$	$\phi 10/12.5cm$
C3	50×50	$12\phi 18$	$\phi 12/5cm$
C4	50×50	$12\phi 18$	$\phi 12/8cm$
C5	40×40	$8\phi 18$	$\phi 12/10cm$
C6	40×40	$8\phi 18$	$\phi 12/12.5cm$
C7	60×60	$16\phi 18$	$\phi 14/5cm$
C8	60×60	$16\phi 18$	$\phi 14/8cm$
C9	50×50	$12\phi 18$	$\phi 14/5cm$
C10	50×50	$12\phi 18$	$\phi 14/8cm$
C11	40×40	$8\phi 18$	$\phi 14/8cm$
C12	40×40	$8\phi 18$	$\phi 14/10cm$
C13	40×40	$8\phi 18$	$\phi 14/12.5cm$

Given the regularity in plan of the examined case-study structures, for each building the design of the hysteretic damper system has been performed on a single internal 2D frame (in line with EC8 §4.2.3—CEN 2004) and considering the tributary loads and masses pertaining to this frame, in line with other studies (Del Gobbo et al. 2018; Karavasilis et al. 2016) and accepted practice.

In order to incorporate the nonlinearity of the parent frame, a concentrated plasticity model for the six frames has been implemented in the software program for structural analysis SAP2000 (CSi, 2017). Automatic hinge properties have been adopted at either end of the structural members, following the recommendations given in ASCE 41–17 (ASCE 2017). In particular, the center of the hinges is located at 5 and 95% of the member length, respectively. Moment-type plastic hinges have been assumed in accordance with Table 9-6 in ASCE 41–17 (ASCE 2017) and ANSI/AISC 360–16 (ANSI/AISC 2016) for steel beams, and in accordance with Table 10-7 in ASCE 41–17 (ASCE 2017) for RC beams. Similarly, coupled axial-moment plastic hinges have been assigned in accordance with Table 9-6 in ASCE 41–17 (ASCE 2017) for steel columns, and with Table 10-8 in ASCE 41–17 (ASCE 2017) for RC columns. The concrete column failure condition has been assigned as condition (ii) in ASCE 41–17 (ASCE 2017), i.e., flexural-shear failure with yielding in flexure occurring before shear failure.

The lateral capacity of the bare frames has been assessed through the nonlinear static (pushover) analysis method under constant gravity loads and monotonically increasing horizontal loads. Two distributions of lateral loads are considered, namely a "modal" pattern (resembling a triangular height-wise profile) and an "uniform" pattern as per EC8 provisions (CEN 2004). The capacity curve (base shear F versus control point displacement d) is obtained for each frame and then processed in accordance with Annex B of EC8 (CEN 2004), as sketched in Fig. 5. The pushover curve (F;d) of the MDOF

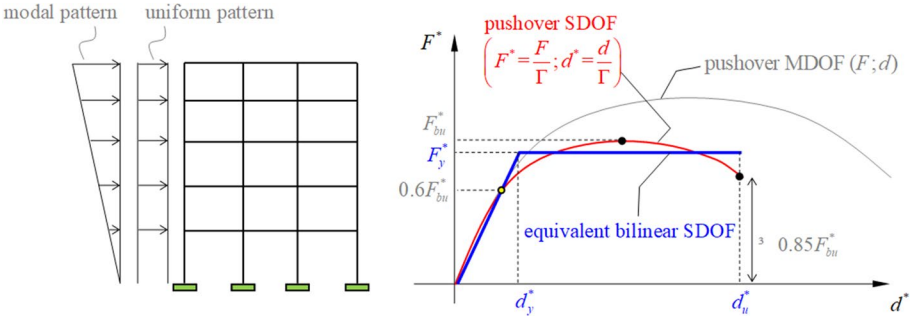

Fig. 5 Determination of equivalent elastic-perfectly plastic SDOF system according to EC8 (CEN, 2004)

system is then scaled by the modal participation factor Γ to obtain the capacity curve F^*-d^* of the equivalent single-degree-of-freedom (SDOF) system $\left(F^*=\frac{F}{\Gamma};d^*=\frac{d}{\Gamma}\right)$. For clarity, hereinafter the quantities with superscript "*" will refer to equivalent SDOF systems, and quantities devoid of suffix will refer to MDOF systems.

The yield force F^*_y and yield displacement d^*_y are determined under the equal energy criterion assuming an ideal elastic-perfectly plastic force–displacement relationship. The yield force $F^*_{y,F}$, yield displacement $d^*_{y,F}$ and ultimate displacement $d^*_{u,F}$ (where subscript $\varepsilon F\varepsilon$ stands for "frame") for the six considered structures are listed in Table 2, along with the modal participation factor Γ and the participating mass m^*. From these values, it is possible to calculate the initial stiffness of the equivalent SDOF model of the bare frame as $k^*_F=F^*_{y,F}/d^*_{y,F}$, the fundamental period $T^*_{1,F}=2\,\pi\sqrt{\frac{m^*}{k^*_F}}$ and the ductility factor $\mu^*_F=d^*_{u,F}/d^*_{y,F}$. These values will be used in the design of the hysteretic dampers, as explained in Sect. 2.3. It is worth noting that the fundamental periods of the equivalent steel frames are much longer than those of the RC frames. This is due not only to the more flexible nature of the steel frame (with a higher inter-storey height and longer bay span) compared to the RC frames, but also to a higher equivalent mass m^* induced by the larger tributary area and by the relatively high loads per unit area (live loads of 3.80 kN/m^2) of the reference steel frames taken from the INNOSEIS project (Vayas et al. 2017). In this regard, this circumstance widens the range of applicability of the results of this numerical study to really flexible structures.

Table 2 Parameters of the elastic-perfectly plastic equivalent SDOF models of case-study frames

Structure	Γ[-]	$T^*_{1,F}$[s]	m^*[ton]	Modal pattern			Uniform pattern		
				$F^*_{y,F}$[kN]	$d^*_{y,F}$[m]	$d^*_{u,F}$[m]	$F^*_{y,F}$[kN]	$d^*_{y,F}$[m]	$d^*_{u,F}$[m]
2-storey steel frame	1.21	1.03	148.33	611.66	0.110	0.413	629.03	0.101	0.413
4-storey steel frame	1.27	2.00	268.30	493.17	0.187	0.628	524.48	0.162	0.528
8-storey steel frame	1.28	4.18	520.97	319.98	0.272	0.474	346.76	0.231	0.390
3-storey RC frame	1.33	0.35	44.08	267.39	0.019	0.270	303.25	0.018	0.254
6-storey RC frame	1.33	0.69	88.33	273.91	0.038	0.377	321.9	0.034	0.377
9-storey RC frame	1.39	0.81	119.12	342.09	0.048	0.358	430.81	0.043	0.358

2.2 Seismic input

The municipality of Lamezia Terme (latitude 38.57°, longitude 16.18°), a city in a high-seismic prone area in southern Italy, has been considered for the design of the supplemental energy dissipation system. Four design response spectra have been defined in accordance with the Italian building code provisions (CSLLPP 2018) for buildings characterized by a nominal life $V_N = 100$ years, and a functional class IV (amplification factor $C_U = 2.0$) resulting in a reference period $V_R = V_N \cdot C_U = 200$ years. Among the four design limit states considered in the code, the "SLD" (return period of 201 years) has been chosen as representative of frequent SLS earthquakes, while the "SLV" (return period of 2475 years) has been selected to represent rare ULS events. Topography condition T_1 has been assumed while, in order to account for different frequency contents of the ground motion, both type A (stiff) and type C (moderate-soft) soils have been considered, resulting in four different design spectra: "ULS-soilA", "ULS-soilC", "SLS-soilA", and "SLS-soilC". Relevant peak ground accelerations are: (1) PGA = 0.452g for "ULS-soilA"; (2) PGA = 0.181g for "SLS-soilA"; (3) PGA = 0.456g for "ULS-soilC"; (4) PGA = 0.261g for "SLS-soilC". For each spectrum, a suite of fourteen independent spectrum-compatible natural records has been extracted (in total 56 events) from the European strong-motion database (Ambraseys et al. 2002) by means of the software REXEL v. 3.5 (Iervolino et al. 2010). For each suite, seven records have been selected among "near-fault" events with epicentral distance $R_{ep} \leq 15km$, and the remaining seven records among "far-field" events with epicentral distance $R_{ep} \geq 30km$. In all cases, the magnitude has been constrained in the range $5 \leq M_w \leq 8$. The selected acceleration time histories have been scaled in order to match, on average, the target design spectrum over the period range [0.15 − 4.00s] (Fig. 6). Seismological details of the selected ground motions are given in Tables 3, 4, 5, 6 of the Annex. It is worth noting that, among the characteristic parameters of the seismic events, the frequency content (through two types of foundation soil), the epicentral distance, and the intensity level (i.e. ULS or SLS) of the seismic event have been explicitly taken into account in this study. However, the cyclic engagement of dissipative braces may depend also on the duration of the ground motion. In this regard, the effect of the "Trifunac duration", i.e. length of the time-window between the release of 5% and 95% of the overall seismic energy (Trifunac et al. 1975), is a matter of concern that deserves future investigations. In this study, as witnessed by values reported in Tables 3, 4, 5, 6, the "Trifunac duration" of the selected ground motion records ranges from 3.4 to 63.8 s, and hence covers from short to long-lasting events.

2.3 Design of the dissipative braces

Each frame has been retrofitted by introducing dissipative braces, consisting of steel braces incorporating hysteretic dampers, as supplemental energy dissipation system.

In the first step of the design procedure of the dissipative system, a target displacement ($d^*_{targ,ULS}$) for the braced frame under ULS seismic events has been defined in order to achieve an assigned ductility factor for the parent frame (μ^*_F). Bare-frame ductility factors ($\mu^*_F = d^*_{targ,ULS}/d^*_{y,F}$) equal to either 1.0 or to a value $\mu^*_F max$ in the range $[1.1 \div 1.6]$ comparable to that assumed in other studies (Di Cesare et al. 2017a). In the first case, identified as "$\mu^*_F = \mu^*_F 1$", the structure behaves elastically and therefore the requested damping force is maximized. In the second case, referred to as "$\mu^*_F = \mu^*_F max$", the damping force is minimized in order to achieve the allowed plastic deformation of the frame.

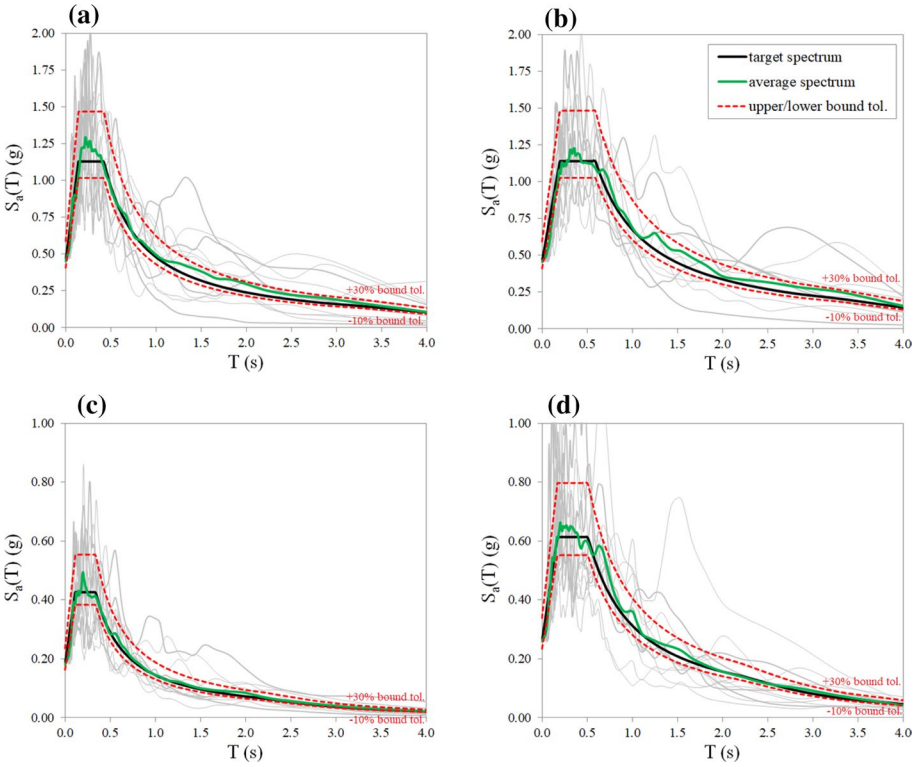

Fig. 6 Comparison between the target spectrum and the average spectrum obtained for each suite of fourteen ground motion records for: **a** ULS-soilA; **b** ULS-soilC; **c** SLS-soilA; **d** SLS-soilC

For the design procedure, three damper ductility factors ($\mu^*_D = d^*_{targ,ULS}/d^*_{y,D}$) have been examined, namely 4 ("μ^*_D4" case), 8 ("μ^*_D8" case), 12 ("μ^*_D12" case). For simplicity, only elastic-perfectly plastic systems will be addressed in the present study, whereas systems with hardening behaviour will be investigated in future developments.

In the second step, the mechanical properties of the dampers are adjusted in order to meet the ULS displacement target. A linear equivalent spectral analysis is carried out where the response of the braced frame is modelled as two equivalent linear SDOF systems working in parallel (Fig. 7-left), representing the parent frame (subscript "*F*") and the damper (subscript "*D*"), respectively. The resulting effective vibration period of the braced frame ($T^*_{eff,F+D}$) is:

$$T^*_{eff,F+D} = 2\pi \sqrt{\frac{m^*}{\left(k^*_{eff,F} + k^*_{eff,D}\right)}} \tag{1}$$

where $k^*_{eff,F} = F^*_{y,F}/d^*_{targ,ULS}$, and $k^*_{eff,D} = F^*_{y,D}/d^*_{targ,ULS}$ are the effective stiffnesses of the bare frame and dissipative bracing system, respectively.

In accordance with (Priestley et al. 2007) for "in parallel systems", the equivalent viscous damping of the braced frame ($\xi^*_{eq,F+D}$) is:

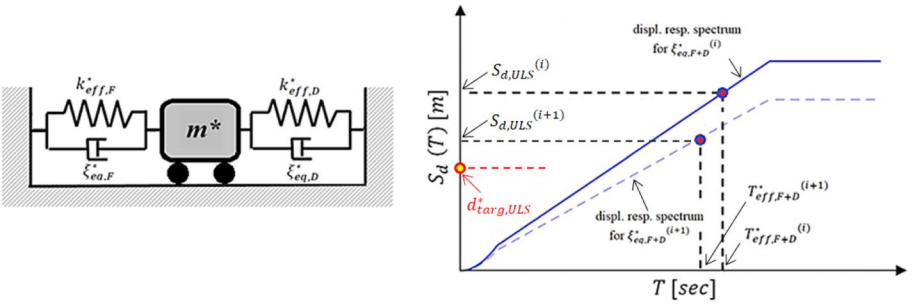

Fig. 7 Adopted design method for the hysteretic damper: rheological model (left) and iterative response spectrum analyses (right)

$$\xi^*_{eq,F+D} = \xi^*_{el,F} + \frac{\xi^*_{eq,F} \cdot F^*_{y,F} + \xi^*_{eq,D} \cdot F^*_{y,D}}{F^*_{y,F} + F^*_{y,D}} \tag{2}$$

being $\xi^*_{el,F}$ the viscous damping of the frame in the elastic range (here conventionally assumed equal to 5%), $F^*_{y,F}$ and $F^*_{y,D}$ the yielding forces of the frame and the damper, respectively, and $\xi^*_{eq,F}$ and $\xi^*_{eq,D}$ the equivalent viscous damping of the frame and the dampers, calculated as (Dwairi et al. 2007):

$$\begin{cases} \xi^*_{eq,F} = \left[85 + 60\left(1 - T^*_{eff,F+D}\right)\right] \cdot \left(\frac{\mu^*_F - 1}{\pi \mu^*_F}\right) & \mu^*_F > 1.0, T^*_{eff,F+DB} < 1,0s \\ \xi^*_{eq,F} = 85 \cdot \left(\frac{\mu^*_F - 1}{\pi \mu^*_F}\right) & \mu^*_F > 1.0, T^*_{eff,F+DB} \geq 1,0s \\ \xi^*_{eq,F} = 0 & \mu^*_F \leq 1.0, \forall T^*_{eff,F+DB} \end{cases} \tag{3}$$

$$\begin{cases} \xi^*_{eq,D} = \left[85 + 60\left(1 - T^*_{eff,F+D}\right)\right] \cdot \left(\frac{\mu^*_D - 1}{\pi \mu^*_D}\right) & \mu^*_D > 1.0, T^*_{eff,F+DB} < 1,0s \\ \xi^*_{eq,D} = 85 \cdot \left(\frac{\mu^*_D - 1}{\pi \mu^*_D}\right) & \mu^*_D > 1.0, T^*_{eff,F+DB} \geq 1,0s \\ \xi^*_{eq,D} = 0 & \mu^*_D \leq 1.0, \forall T^*_{eff,F+DB} \end{cases} \tag{4}$$

It is worth noting that numerical value of $\xi^*_{eq,F+D}$ never exceeds 0.24 (i.e. 24% of the critical damping) even for the largest damper ductility ratio (i.e. $\mu^*_D = 12$) considered in this study. Therefore, the ratio between the "damped" ($T^{*(damp)}_{eff,F+D}$) and "undamped" ($T^*_{eff,F+D}$) fundamental periods of the braced frames $T^{*(damp)}_{eff,F+D}/T^*_{eff,F+D} = 1/\sqrt{1 - (\xi^*_{eq,F+D})^2}$ is always lower than 1.03. This means that the hysteretic damping introduced by the dampers has a negligible ($\leq$3%) influence on the fundamental period of the braced frames. Based on these considerations, the adoption of the undamped natural period of the braced frame is a reasonable simplification in this design procedure.

Within a recursive procedure, the yield force of the damper ($F^*_{y,D}$) is iteratively adjusted (Fig. 7, right) until the spectral displacement of the braced frame converges to the design target, i.e. $\left|S_{d,ULS}\left(T^*_{eff,F+D},\ \xi^*_{eq,F+D}\right)^{(i)} - d^*_{targ,ULS}\right| \leq 0.01 \cdot d^*_{targ,ULS}$. At the generic *ith* iteration, corresponding to a pair of parameters $\left(T^*_{eff,F+D}{}^{(i)}, \xi^*_{eq,F+D}{}^{(i)}\right)$ the spectral displacement

of the braced frame is obtained through the spectral reduction factor (η) proposed in (Priestley et al. 2007):

$$\begin{cases} S_{d,ULS}\left(T^{*(i)}_{eff,F+D},\ \xi^{*(i)}_{eq,F+D}\right) = \frac{1}{\eta^{(i)}} \cdot S_{d,ULS}\left(T^{*(i)}_{eff,F+D},\ 5\%\right) \\ \eta^{(i)} = \sqrt{7/\left(2+\xi^{*(i)}_{eq,F+D}\right)} \end{cases} \quad (5)$$

being $S_{d,ULS}\left(T^{*}_{eff,F+D}{}^{(i)}, 5\%\right)$ the ULS elastic displacement at 5% damping for period $T^{*}_{eff,F+D}{}^{(i)}$.

It is worth noting that Eqs. 3 and 4 overcome the inherent error of the conventional approach based on the Jacobsen formulation (Jacobsen, 1930) that typically overestimates the equivalent damping ratio of medium-to-long period hysteretic systems (Mazza et al. 2015a). Moreover, it was found that the proposed approach, in combination with the adopted spectral reduction factor (Eq. 5-b), guarantee the best accuracy in the prediction of peak displacements of a wide range of inelastic systems (Casarotti et al. 2009).

The resulting design parameters of the seventy-two equivalent SDOF systems are reported in Tables 7 and 8 of the Annex. Each equivalent SDOF system is identified by an alphanumeric string coded as follows: (a) "rc3", "rc6", and "rc9" stand for reinforced concrete frame with three, six, or nine storeys, respectively; (b) "st2", "st4", and "st8" stand for steel frame with two, four, or eight storeys, respectively; (c) "sA" and "sC" mean soil type A and type C, respectively; (d) "μ^{*}_{F}1" and μ^{*}_{F}max stand for parent frame target ductility factor $\mu^{*}_{F} = 1.0$ and $\mu^{*}_{F} > 1.0$, respectively; (e) "μ^{*}_{D}4", "μ^{*}_{D}8", and "μ^{*}_{D}12" are used for damper ductility factor μ^{*}_{D} equal to 4, 8, and 12, respectively. It should be noted that for cases "st2-sA-μ^{*}_{F}max-μ^{*}_{D}4", "st2-sA-μ^{*}_{F}max-μ^{*}_{D}8", and "st2-sA-μ^{*}_{F}max-μ^{*}_{D}12", corresponding to two-storey steel frames on soil A, the target ductility of the frame μ^{*}_{F}max > 1 was achieved without introducing any suplemental damper, as shown in (Fig. 8). In fact, by comparing the "sA" design spectrum and "st2" frame capacity curve in the ADRS plane (ATC 1996) and assuming a target frame ductility μ^{*}_{F}max = 1.1, even disregarding any supplemental energy dissipation, the damping

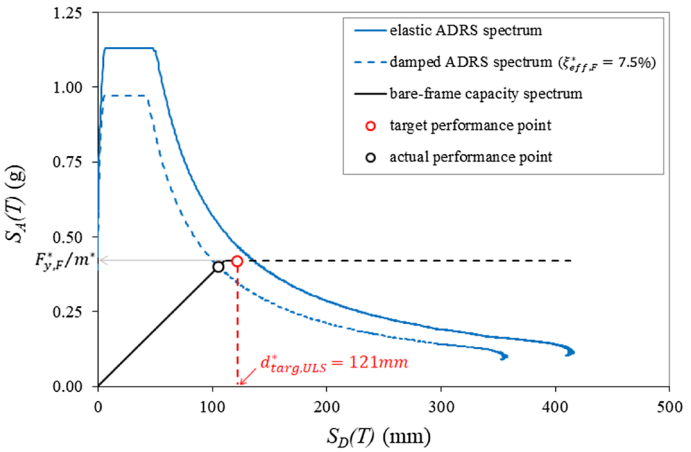

Fig. 8 Identification of the actual performance point through the ADRS representation of the "sA" response spectrum and "st2" capacity curve

provided by the bare-frame ($\xi^*_{eff,F} = \xi^*_{el,F} + \xi^*_{eq,F} = 7.5\%$) is enough to achieve the target displacement ($d^*_{targ,ULS} = 1.1 \bullet d^*_{y,F} = 121\text{mm}$).

The method followed to distribute the damping force ($F^*_{y,D}$), and elastic stiffness ($k^*_{el,D}$) of the equivalent SDOF damper along the various storeys of the MDOF frame is in accordance with previous literature studies (Ponzo et al. 2010; Di Cesare et al. 2014; 2017a). By referring to the installation layout shown in Fig. 9-a, with dampers arranged in a reverse-V bracing configuration at each storey, the yielding force of the units at the generic i^{th} storey is:

$$F_{y,D(i)} = \left(\frac{F_{y,F(i)}}{F^*_{y,F}}\right)\left(\frac{F^*_{y,D}}{n_{D(i)} \cdot cos\vartheta_{(i)}}\right) \tag{6}$$

being: (1) $n_{D(i)}$ the number of units at the considered storey (for sake of simplicity, in the specific case $n_{D(i)} = 1$); (2) $\vartheta_{(i)}$ the angle between the line of action of the damper's output force and the horizontal direction (in the specific case $\vartheta_{(i)} = 0°$); (3) $F_{y,F(i)}$ the overall lateral yield force of the frame columns at the i^{th} storey. The same approach has been also adopted for the calculation of the elastic stiffness of the damper units:

$$k_{el,D(i)} = \left(\frac{k_{el,F(i)}}{k^*_{el,F}}\right)\left(\frac{k^*_{el,D}}{n_{D(i)} \cdot cos^2\vartheta_{(i)}}\right) \tag{7}$$

being $k_{el,F(i)}$ the elastic stiffness for horizontal forces of the parent frame columns at the *i*th storey.

For simplicity, the stiffness of the damped brace has been assumed to coincide in practice with the stiffness of the hysteretic damper, i.e. the brace rods used to link the damper to the structural frame are very stiff and, under the actions induced by the design earthquake, undertake very small deformations in comparison to the damper's ones. Otherwise, a simple approach to account for the flexibility of link elements can be found in the aforementioned studies (Ponzo et al. 2010; Di Cesare et al. 2014; 2017a).

3 Equivalent SDOF model for NLTH analyses

The design of the damping system necessary to achieve the target seismic performance for the frame is performed by spectral analyses considering equivalent SDOF models, according to accepted practice (Ponzo et al. 2010; Di Cesare et al. 2017a; Mazza et al. 2015a; 2015b; Bergami et al. 2013). Hence, it is interesting to investigate if equivalent SDOF models (Fig. 9-b) can be employed also in NLTH analyses as a simplified alternative to MDOF models (Fig. 9-a), allowing a significant saving of computational effort and data post-processing times. In the analyses of the MDOF system, hysteretic dampers have been modelled as nonlinear shear links (two-DOF MultiLinear Plastic NL-Link elements in SAP2000—CSI 2017) with an elastic-perfectly plastic force–displacement behavior, connected to the frame though very stiff beam elements reproducing a chevron (or "reversed V") brace configuration. Such configuration has been adopted because of its simplicity and suitability to provide a direct relationship between the damper force and the structure inter-storey drift; however, alternative configurations, like e.g., diagonal braces, can be implemented in the model as well. The equivalent SDOF model has been formulated in OpenSees software program for structural analysis (McKenna et al. 2000) by means of

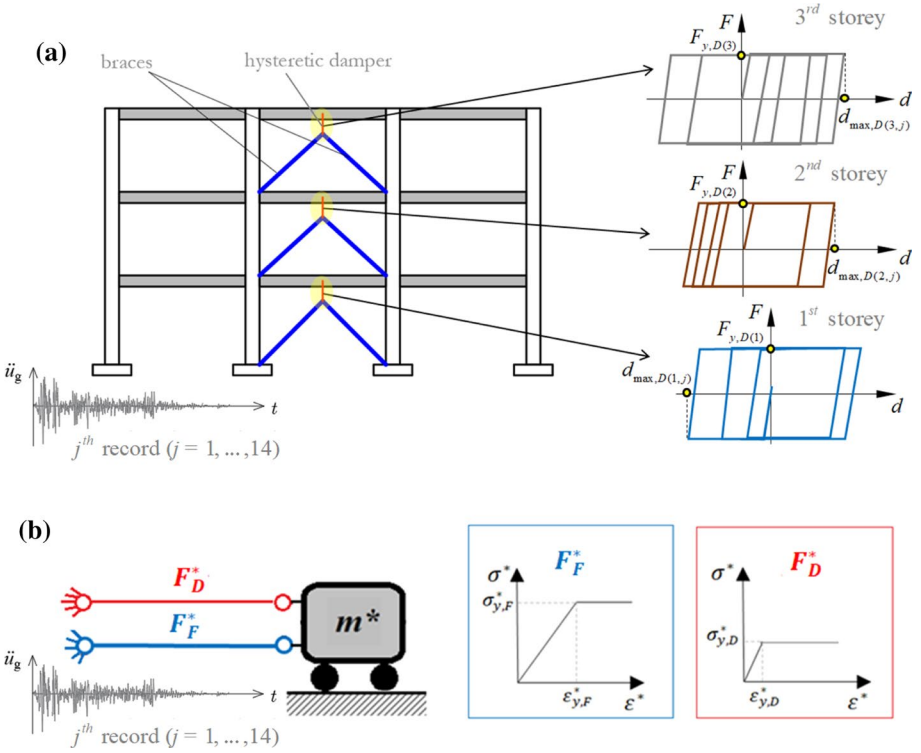

Fig. 9 Structural models adopted in NLTH analyses: **a** MDOF braced frame (with a scheme of the calculation method for the number of effective cycles of the damper); **b** equivalent SDOF system

two elastic-perfectly plastic truss elements working in parallel, representing the equivalent SDOF bare-frame and the equivalent SDOF damper, respectively.

For brevity, nonlinear SDOF time-history analyses (NLTHs) have been assessed considering only "extreme" configurations of damped braced frames, and assuming that the ensuing validation envelopes the intermediate cases. Validation cases include hence: (a) the stiffest ("rc3", $T^*_{1,F} = 0.35s$) and the most flexible ("st8", $T^*_{1,F} = 4.18$s) frame; (b) damper ductility factor $\mu^*_D = 4$ or $\mu^*_D = 12$; (c) target ductility factor of the braced frame μ^*_F=1.0 or $\mu^*_F = \mu^*_{F,max} > 1.0$. A total of 224 NLTH analyses have been carried out: 112 analyses of MDOF systems, and 112 analyses of equivalent SDOF systems.

For each braced frame, the maximum displacement at roof level of the MDOF system, $d^{\mathrm{MDOF}}_{\max}$, has been calculated as the average of the peak roof displacements induced by the fourteen ground motion records; this value has been compared (Fig. 10-a) to the maximum displacement of the equivalent SDOF model obtained either by a spectral analysis ($d^{\mathrm{spec}}_{\max}$) or by nonlinear time history analyses, $d^{\mathrm{SDOF}}_{\max}$, multiplied times the modal participation factor Γ. As expected, the "rc3" systems experience much smaller lateral deformations ($d^{\mathrm{MDOF}}_{\max} = 23 \div 37$ mm) than "st8" systems ($d^{\mathrm{MDOF}}_{\max} = 324 \div 396$ mm). The relative deviation between peak displacements predicted by spectral analyses considering the equivalent SDOF system and peak displacements from NLTHs of the MDOF system ($\Delta_{\%} = 100 \bullet (\Gamma d^{\mathrm{spec}}_{\max} - d^{\mathrm{MDOF}}_{\max})/d^{\mathrm{MDOF}}_{\max}$) is between −1.1 and + 10.6% in seven out of eight cases, with only a case where the deviation is + 25.0%, resulting in an average error of + 8.5% (Fig. 10-b). For NLTH analyses with the equivalent SDOF system

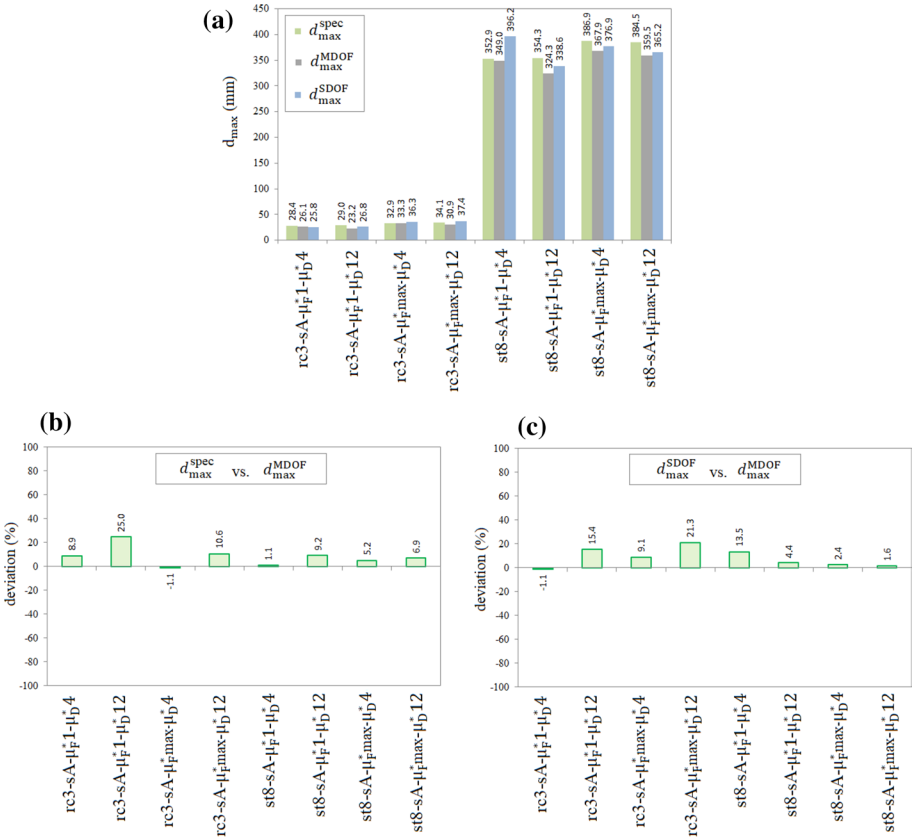

Fig. 10 **a** Comparison between peak displacement calculated through spectral, MDOF, and equivalent SDOF NLTH analyses; **b** accuracy of spectral analyses; **c** accuracy of equivalent SDOF NLTH analyses

(Fig. 10-c), the relative deviation ($\Delta_{\%} = 100 \bullet (\Gamma d_{max}^{SDOF} - d_{max}^{MDOF})/d_{max}^{MDOF}$) lies between −1.1 and + 15.4% in seven out of eight cases, with a single case reaching a + 21.3% deviation, and the average error is + 8.6%. On average, the accuracy of the SDOF models seems to be worse for stiff buildings ("rc3" cases) and high ductility dampers ("μ_D^* = 12"). Based on these results, it can be concluded that equivalent SDOF models can be used with sufficient reliability (average error less than 10%) to perform either liner equivalent spectral analyses or NLTH analyses for the prediction of the maximum seismic displacement of MDOF braced frames.

Since during real earthquakes the displacement histories which the dissipating devices are subjected to are generally not symmetric, an "effective cycle" has been defined based on the equivalence of dissipated energy between the actual force—displacement cycle and the theoretical cycle shown in Fig. 1. The number of effective cycles N_{cycles} performed by the hysteretic damper during a ground motion is defined by Eq. (8):

$$N_{cycles} = \frac{E_{diss}(d_{max,D})}{4 \cdot \left[\left(F_{y,D} \cdot d_{\max,D}\right) - \left(F_{y,D} \cdot d_{y,D}\right)\right]} \tag{8}$$

where $E_{diss}(d_{max,D})$ is the hysteretic energy dissipated by the damper over the actual displacement history with maximum displacement $d_{max,D}$, and $4 \bullet \left[\left(F_{y,D} \bullet d_{\max,D}\right) - \left(F_{y,D} \bullet d_{y,D}\right)\right]$ is the energy dissipated by the damper in an ideal (symmetric) cycle with extreme displacements $\pm d_{max,D}$.

The number of effective cycles will be used hereinafter to evaluate the cyclic engagement of the damper.

For the braced frame, the number of effective cycles of the dampers at the *i*th storey under the application of the *j*th ground motion is calculated as:

$$N_{cycles}^{MDOF\ (i,j)} = \frac{E_{diss}^{(i,j)}}{4 \cdot \left[\left(F_{y,D\ (i)} \cdot d_{\max,D(i,j)}\right) - \left(F_{y,D\ (i)} \cdot d_{y,D(i)}\right)\right]} \qquad (i = 1, \ldots, n; j = 1, \ldots, 14) \tag{9}$$

where $F_{y,D\ (i)}$ and $d_{\max,D(i,j)}$ are the yield force and the maximum displacement of the damper at the *i*th storey as shown in the example in Fig. 9(a). A single value of $\bar{N}_{cycles}^{MDOF\ (j)}$ is then calculated for the whole bracing system of the frame as the average of the values in Eq. 9 relevant to the n storeys, and then both the average (N_{cycles}^{MDOF}) and the 90th percentile value ($N_{cycles,90\%}^{MDOF}$) are calculated considering the ensemble of 14 spectrum-compatible ground-motion records. The comparison among the results is shown in Fig. 11-left. Although this trend should be confirmed through a wider parametric study (Sect. 4), it is clearly seen that bracing systems used in stiffer frames, i.e. "rc3"cases, are characterized by a higher number of effective cycles ($N_{cycles} = 2.9 \div 6.1$, $N_{cycles,90\%} = 4.6 \div 10.6$) than bracing systems used in more flexible "st8" frames ($N_{cycles} = 1.0 \div 2.2$, $N_{cycle,90\%} = 1.7 \div 3.8$). The accuracy of NLTH analyses using equivalent SDOF systems in predicting N_{cycles} is shown in Fig. 11-right: the relative deviation ($\Delta_{\%} = 100 \cdot \left(N_{\text{cycles}}^{\text{SDOF}} - N_{\text{cycles}}^{\text{MDOF}}\right)/N_{\text{cycles}}^{\text{MDOF}}$) ranges between -18.1% and +9.1% in seven out of eight cases, with a single case reaching -23.6%. The same comparison is shown for $N_{cycle,90\%}$ in Fig. 12: the relative deviation ($\Delta_{\%} = 100 \cdot \left(N_{\text{cycles,90\%}}^{\text{SDOF}} - N_{\text{cycles,90\%}}^{\text{MDOF}}\right)/N_{\text{cycles,90\%}}^{\text{MDOF}}$) ranges between -19.5% and +10.7% in

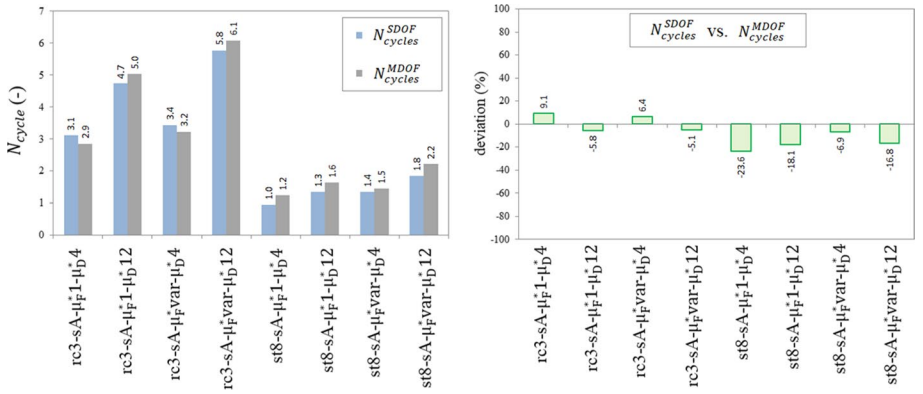

Fig. 11 Comparison between the number of effective cycles sustained by hysteretic dampers (N_{cycles}) calculated in NLTH analyses using either MDOF models or equivalent SDOF-NLTH models (left), and relative deviation (right)

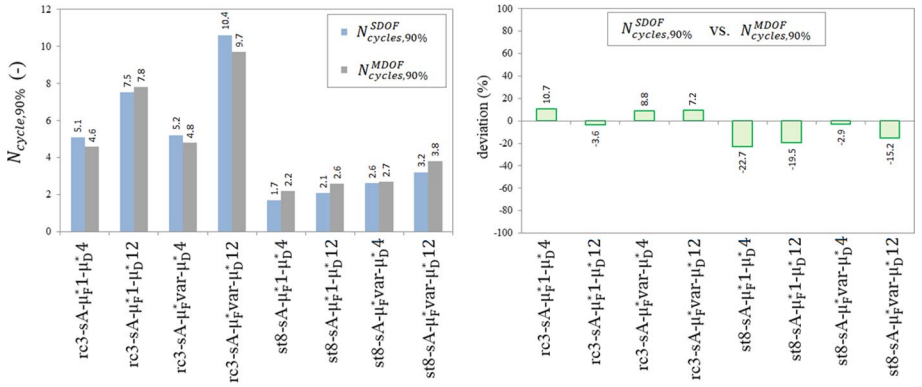

Fig. 12 Comparison between the 90th percentile of number of effective cycles sustained by hysteretic dampers ($N_{cycles,90\%}$) calculated in NLTH analyses using either MDOF models or equivalent SDOF models (left), and relative deviation (right)

seven out of eight cases, with a single case reaching -22.7%. It is worth noting that the highest deviations are achieved for the "st8" configuration which, on the other side, represents the less critical case since, on average, subjected to minimum cyclic engagement. Moreover, as shown in Fig. 13, the deviation between $N^{\mathrm{SDOF}}_{\mathrm{cycles},90\%}$ and $N^{\mathrm{MDOF}}_{\mathrm{cycles},90\%}$ tends to vanish when the number of effective cycles is rounded to the closest integer: only in two cases (among those relevant to the less demanding "st" layouts) a discrepancy of 1 cycle (which is deemed to be acceptable) is found. However, based on these preliminary results, in order to encompass the effects of all possible uncertainties associated to the use of simplified

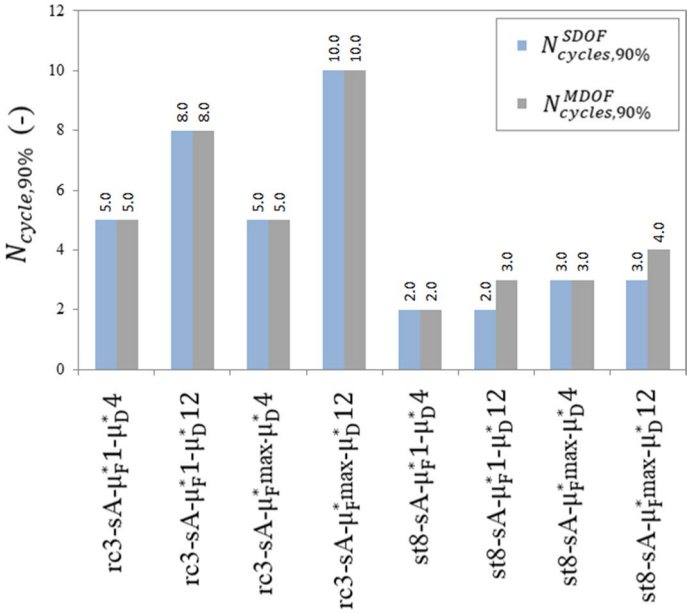

Fig. 13 Comparison between rounded values of $N^{\mathrm{SDOF,NLTH}}_{\mathrm{cycles},90\%}$ and $N^{\mathrm{MDOF,NLTH}}_{\mathrm{cycles},90\%}$

equivalent SDOF analyses, the "reliability factor" $\gamma_X = 1.25$ will be later introduced when a dedicated relationship to predict the number of effective cycles experienced by hysteretic dampers is formulated.

4 Results of the parametric investigation

The effective cycles sustained by hysteretic dampers have been investigated by means of NLTH analyses on equivalent SDOF models, as justified by the validation presented in Sect. 3. The 72 examined braced frame configurations (Tables 7 and 8) have been subjected to the applications of 14 ground motions at SLS (Tables 3 and 5) and 14 ground motions at ULS (Tables 4 and 6) resulting in a total of 2008 NLTH analyses. The cyclic engagement of the equivalent SDOF damper is calculated in each analysis and then statistically processed. The cyclic engagement, which according to Eq. (8) is associated to the amount of dissipated energy during the seismic movement, depends both on the overall lateral flexibility of the braced frame (as anticipated in Sect. 3) and on the "pulse-like" characteristics of the seismic input. Very high values of N_{cycles} are indeed calculated for stiff structures subjected to far-field ($R_{ep} > 30km$) events while, on the contrary, low values of N_{cycles} are observed for flexible structures experiencing near-fault ($R_{ep} < 15km$) ground motions. This is evident in Fig. 14 that compares the displacement histories of two braced frames presenting the largest ($N_{cycles} = 17.4$) and the smallest ($N_{cycles} = 1.1$) number of effective cycles. The peak lateral displacement of the stiff "rc3" system subjected to the far-field "ulsC-13" ground motion exceeds several times the yield limit of the damper; on the contrary, the flexible "st8" system subjected to the near-fault "ulsC-4" event experiences a single large "pulse-like" movement, and, afterwards, the yield limit of the damper ($d^*_{y,D}$) is slightly exceeded only three more times.

The effective viscous damping of the braced frame seems not to have a clear influence on the cyclic engagement of the damper, as shown in Fig. 15 that reports the number of effective cycles (N_{cycles}) as a function of the effective viscous damping $\xi^*_{eq,F+D}$ for each examined structural system and each ground motion.

On the contrary, a direct relation exists between the number of cycles, the effective period of the braced frame $T^*_{eff,F+D}$ and the frequency content of the seismic input. A synthetic index is therefore introduced as follows:

$$\hat{T} = \frac{T^*_{eff,F+D}}{T_C} \tag{10}$$

where T_C is the transition period between the constant acceleration and the constant velocity branches of the ULS spectrum (equal to either 0.42 or 0.59 s for soil type A or type C, respectively).

In Fig. 16 the number of effective cycles (N_{cycles}) calculated, for each case, as the average value over the 14 ground motions, is plotted as a function of $\widehat{T}$. Each plot contains 144 data-points grouped in twelve classes that differ for: (a) the parent frame; and (b) the epicentral distance (R_{ep}) of the seismic input. By analysing the trend-line enveloping all data points, a logarithmic decrease of N_{cycles} is noticed. By considering ULS events (Fig. 16-left), N_{cycles} is as high as 9.4 for stiff "rc3" frames with $\widehat{T} < 1.0$ and reduces to 2.7 for flexible "st8" frames with $\widehat{T} > 9.0$. The epicentral distance (R_{ep}) also seems to have a certain influence: data points corresponding to $R_{ep} < 15$ km are in general located below data points corresponding to $R_{ep} > 30$ km, highlighting a slightly

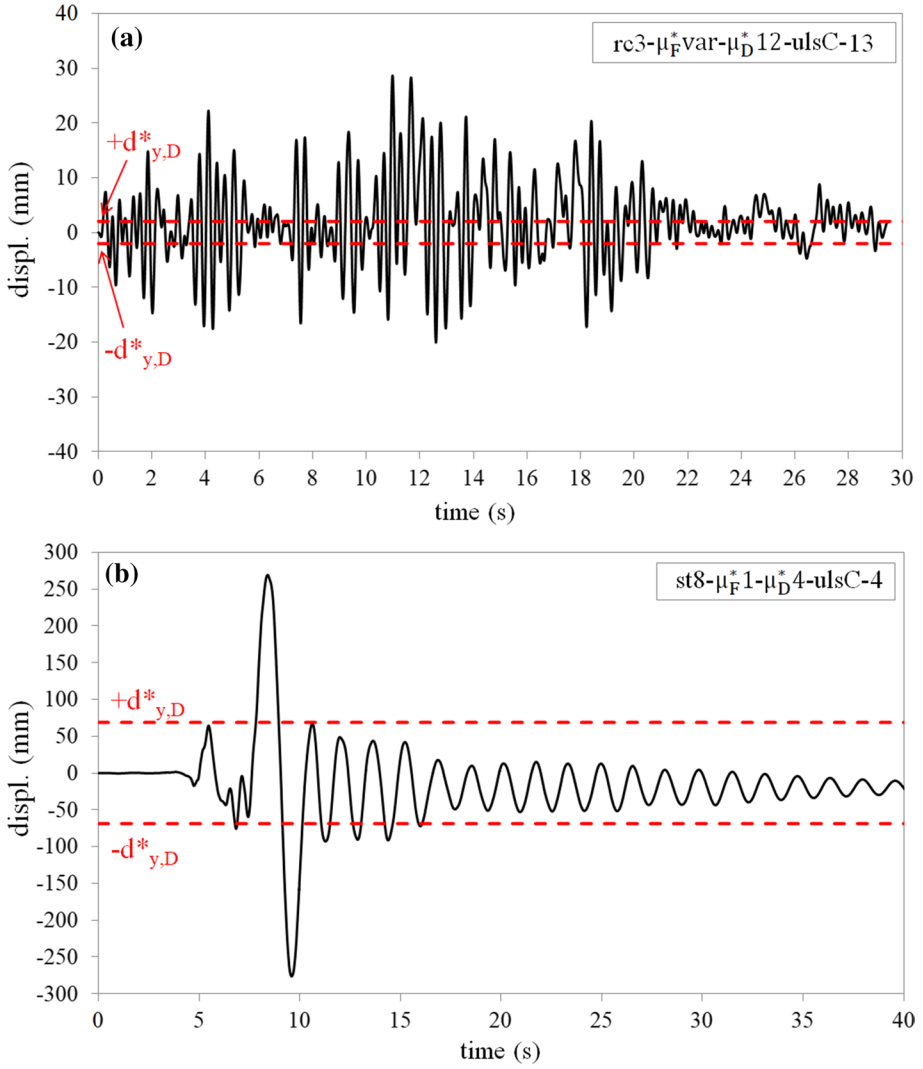

Fig. 14 Comparison between the displacement time-histories of the "$F^* + D^*$" systems with a large (**a**) and a small (**b**) hysteretic engagement

lower cyclic engagement in case of near-fault ground motions compared to far-field ground motions. This phenomenon is probably caused by the intrinsic oscillatory nature of the latter events while the former are often characterized by "pulse-like" behaviour (Guo et al. 2018; Baker, 2007). Nevertheless, the dependence on R_{ep} seems to be weaker than that on $\widehat{T}$ and this relationship should be investigated in more details by considering a wider set of ground motion records.

A very close trend is noticed when SLS seismic inputs are considered (Fig. 16-right). As expected, a lower cyclic engagement of the equivalent damper is determined; indeed, the logarithmic envelope curve decreases from 6.4, when $\widehat{T} < 1.0$, to 1.8, when $\widehat{T} > 9.0$.

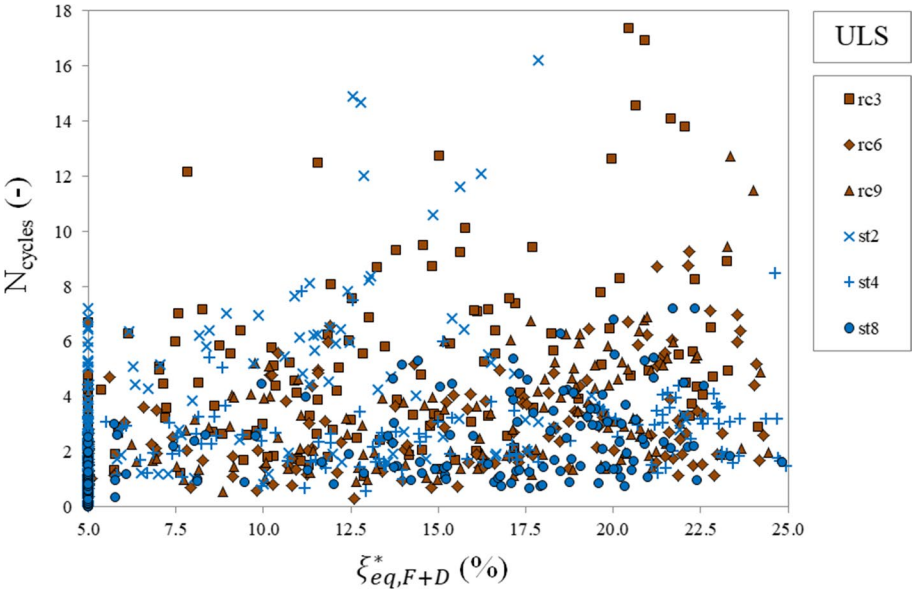

Fig. 15 Damper cyclic engagement (N_{cycles}) at ULS as a function of the equivalent viscous damping ($\xi^*_{eq,F+D}$) of the braced frames

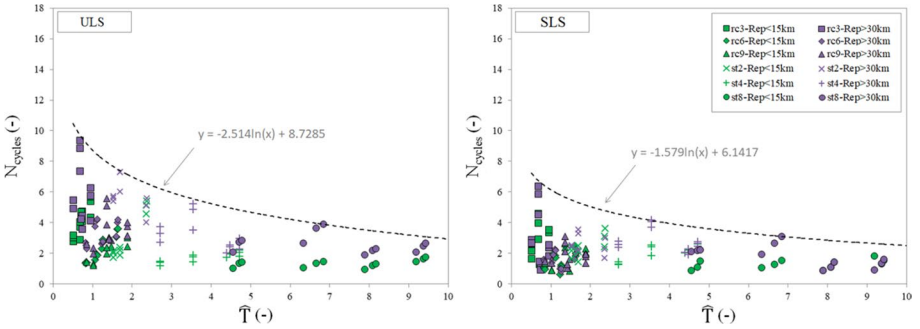

Fig. 16 Damper cyclic engagement (N_{cycles}) at ULS (left) and SLS (right)

In Fig. 17 the 90th percentile of the number of effective cycles ($N_{cycles,90\%}$) at ULS and SLS is shown. Either panel contains 72 data-points grouped into six categories based on the parent frame. Each value of $N_{cycles,90\%}$ has been calculated over a set of 14 NLTHs including both near-fault and far-field events. For ULS events, $N_{cycles,90\%}$ is as high as 14.4, when $\hat{T} < 1.0$, and decreases down to 5.2, when $\hat{T} > 9.0$. All data points are again enveloped by a logarithmic curve, as shown in Fig. 17-left. A logarithmic enveloping function can be plotted also for SLS events (Fig. 17-right): here $N_{cycles,90\%}$ decreases with the increasing of $\hat{T}$ moving from 13.9 for $\hat{T} = 0.68$ to 4.1 for $\hat{T} = 9.4$. It is to be noted that when the 90th percentile of data points is considered, the enveloping curves at ULS and SLS are very close to each other and tend to overlap, suggesting that a single model can be used to relate (see Eq. 11) the cyclic engagement to the governing parameter $\hat{T}$.

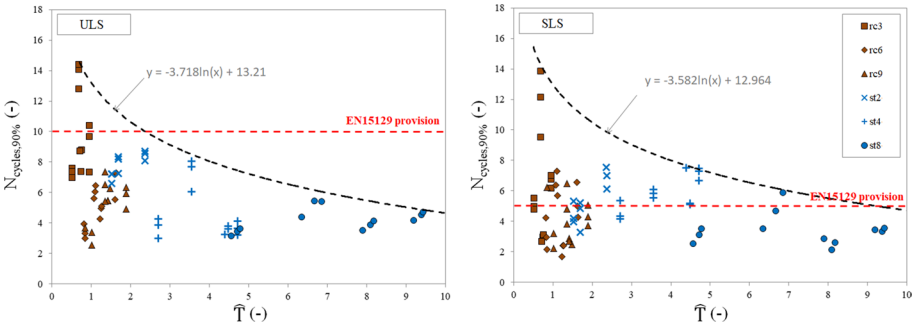

Fig. 17 90th percentile of the number of effective cycles ($N_{cycles,90\%}$) at ULS (left) and SLS (right) seismic events

4.1 Assessment of the EN15129 provisions

The results are now used to evaluate the suitability of the testing protocol (Fig. 2) recommended in the European standard EN15129 (CEN 2009). The two series of 5 cycles at 25% (run 1) and 50% (run 2) of the design displacement d_{bd} are intended to assess the effective stiffness and damping of the device for low and medium intensity earthquakes, corresponding to SLS events, while the 10 cycles at 100% d_{bd} (run 3) are intended to assess the degradation of mechanical properties (namely, stiffness and damping factor) and the low-cycle endurance of the device subjected to the ULS earthquake. The number of ten cycles should be strictly pertaining to applications producing fundamental periods of the order of 2 s, whereas if the fundamental period of the structural system is considerably less than 2 s, the code prescribes to increase the number of cycles according to the Structural Designer's specifications.

The results of the present study highlight that the number of effective cycles sustained by the hysteretic damper is also affected by the spectral characteristics of the seismic input through the transition period T_C which is used for the calculation of $\widehat{T}$. The 10 cycles prescribed in the standards turn out to be appropriate for $3.0 < \widehat{T} < 7.0$, i.e., for applications in flexible frames (e.g., medium-rise steel frames), but extremely demanding for $\widehat{T} > 7.0$, when the number of effective cycles is lower or at the most equal to six. In contrast, for applications to stiff frames (e.g., low-rise RC frames) ten cycles appear to be under-conservative to assess the cyclic behavior of the damper, underestimating by a factor up to 1.5 the actual engagement. Eventually, run 1 plus run 2 do not appear to be appropriate to simulate the cyclic engagement of DDDs under SLS earthquakes in case of devices installed in rigid frames. In fact, as shown in Fig. 17-right minor earthquakes can trigger up to 14 cycles in braced frames characterized by $\widehat{T} < 1.0$.

Based on the regression equation shown in Fig. 17, the number of symmetric cycles at $\pm d_{bd}$ to be imposed on the test specimen during the tests $N_{cycles,test}$ can be estimated, both at ULS and SLS, by the following expression:

$$\begin{cases} N_{cycles,test} = round\left(N_{cycles,90\%}\right) \\ N_{cycles,90\%} = \gamma_x \cdot \left(-3.7 \ln\left(\widehat{T}\right) + 13.2\right) \end{cases} \tag{11}$$

being: (a) $\gamma_x = 1.25$ a "reliability factor" (as suggested in Sect. 3); (b) "*round*" a function that rounds a decimal number to the closest integer.

It should be noted that the calculation of $N_{cycles,test}$ is straightforward and does not require any computation in addition to those already performed for the design of the dampers, because the only parameters needed for the calculation of $\widehat{T}$ are the effective period of the equivalent SDOF of the braced frame $T^*_{eff,F+D}$ and the transition period T_C of the design spectrum at ULS.

5 Conclusions

The study investigates, through a parametric study, the cyclic engagement of hysteretic dampers (defined as the number of symmetric cycles at the design displacement which provides the same energy dissipation during a design earthquake) used in typical steel or reinforced concrete buildings, in order to ascertain the effectiveness of current testing protocols for qualification and acceptance tests recommended in the European standard EN 15129 (CEN 2009).

The main results of the study are summarized as follows:

- The number of effective cycles sustained by hysteretic dampers installed in a MDOF frame can be assessed through NLTH analyses carried out on an equivalent SDOF model with a reasonable level of accuracy. Indeed the deviation between N^{MDOF}_{cycles} and N^{SDOF}_{cycles} is always lower than 25% and becomes negligible when the relevant values are rounded to the closest integer number;
- The cyclic engagement of the dampers depends on the ratio ($\widehat{T}$) between the effective period of the braced frame ($T^*_{eff,F+D}$) and the transition period (T_C) between the constant acceleration and the constant acceleration branches of the ULS design spectrum. A minor dependence on the "pulse-like" nature of the seismic input has been highlighted; indeed, given a certain value of $\widehat{T}$, far-field events result in a higher N_{cycles} values compared to near-fault ground motions;
- At ULS, the provisions of the standard appear over-conservative for dampers installed in flexible structures but under-conservative when the dampers are installed in stiff structures. Indeed, the number of 10 cycles turns out to be appropriate for $3.0 < \widehat{T} < 7.0$, i.e., for applications to flexible frames (e.g., in medium-rise steel frames), but extremely demanding for $\widehat{T} > 7.0$, when the number of effective cycles is lower than or at the most equal to six. In contrast, for applications to stiff frames (e.g., low rise RC frames), ten cycles appear to be non-conservative, underestimating the actual engagement of the damper up to 50%;
- Also at SLS, the provisions of the standard do not appear to be appropriate in case of devices installed in rigid frames characterized by $\widehat{T} < 1.0$ where the engagement involves up to 14 effective cycles;
- A simple rule to establish the number of cycles to be imposed to the test specimens during the test has been proposed based on the 90th percentile regression equation. This expression is simple, valid for both SLS and ULS estimations and does not require any further computation in addition to those already performed for the design of the dampers.

Eventually, it must be noted that the present work has addressed elastic-perfectly plastic dampers only, which is a reasonable assumption in view of experimental evidence of steel hysteretic dampers featuring post-stiffness ratios not exceeding 10% typically. However, in future developments of this investigation the effects of the post-yielding hardening of steel dampers on their cyclic engagement in braced frames will be assessed.

Appendix

See Tables 3, 4, 5, 6, 7, 8, 9, 10.

Table 3 Details of selected ground motions for Lamezia site, SLS limit state, soil type A

Label	Earthquake name	Wave ID	EQ ID	Station ID	Date	M_w	Fault mech	R_{ep} [km]	PGA [m/s^2]	DUR [s]	D_{Tr} [s]	S.F. [-]
slsA-1	Bingol	7142ya	2309	ST539	01/05/2003	6.3	Strike slip	14	2.9178	64.71	17.30	0.609
slsA-2	Izmit (aftershock)	1243xa	473	ST575	13/09/1999	5.8	Oblique	15	0.7138	19.12	11.26	2.488
slsA-3	Tabas	182ya	87	ST54	16/09/1978	7.3	Oblique	12	3.7789	39.96	34.77	0.470
slsA-4	South Iceland (aftershock)	6335ya	2142	ST2557	21/06/2000	6.4	Strike slip	15	1.1322	57.99	9.84	1.569
slsA-5	Lazio Abruzzo (aftershock)	383xa	176	ST153	11/05/1984	5.5	Normal	14	0.1983	18.16	14.88	8.957
slsA-6	NE of Banja Luka	5655xa	1825	ST2950	13/08/1981	5.7	Oblique	10	0.7302	24.92	13.14	2.432
slsA-7	Izmit	1231xa	472	ST575	17/08/1999	7.6	Strike slip	9	1.5764	51.98	34.07	1.127
slsA-8	South Iceland	6269xa	1635	ST2497	17/06/2000	6.5	Strike slip	34	0.3856	94.69	54.38	4.606
slsA-9	Tithorea	551xa	260	ST212	18/11/1992	5.9	Normal	37	0.1599	10.89	8.71	11.109
slsA-10	South Iceland	6262xa	1635	ST2496	17/06/2000	6.5	Strike slip	31	0.54	57.97	31.64	3.289
slsA-11	South Iceland	6272ya	1635	ST2568	17/06/2000	6.5	Strike slip	42	0.409	50.99	22.38	4.343
slsA-12	Montenegro (aftershock)	234xa	108	ST68	24/05/1979	6.2	Thrust	30	0.6669	24.56	17.19	2.663
slsA-13	South Iceland	4678ya	1635	ST2557	17/06/2000	6.5	Strike slip	32	0.5238	69.99	32.87	3.390
slsA-14	Lazio Abruzzo	369xa	175	ST109	07/05/1984	5.9	Normal	44	0.3512	22.74	12.99	5.057

Table 4 Details of selected ground motions for Lamezia site, ULS limit state, soil type A

Label	Earthquake name	Wave ID	EQ ID	Station ID	Date	M_w	Fault mech	R_{ep} [km]	PGA [m/s^2]	DUR [s]	D_{Tr} [s]	S.F. [-]
ulsA-1	South Iceland	4675xa	1635	ST2487	17/06/2000	6.5	Strike slip	13	1.2916	66.99	6.86	3.434
ulsA-2	South Iceland (aftershock)	6335xa	2142	ST2557	21/06/2000	6.4	Strike slip	15	1.2481	57.99	7.37	3.554
ulsA-3	Bingol	7142ya	2309	ST539	01/05/2003	6.3	Strike slip	14	2.9178	64.71	17.30	1.520
ulsA-4	South Iceland (aftershock)	6326ya	2142	ST2496	21/06/2000	6.4	Strike slip	14	1.1423	42.47	9.89	3.883
ulsA-5	Izmit	1231xa	472	ST575	17/08/1999	7.6	Strike slip	9	1.5764	51.98	34.07	2.814
ulsA-6	Valnerina	242xa	115	ST225	19/09/1979	5.8	Normal	5	1.5095	24.98	10.95	2.938
ulsA-7	Mt. Hengill Area	5085xa	1464	ST2497	04/06/1998	5.4	Strike slip	15	0.1199	42.22	8.47	36.992
ulsA-8	South Iceland	6269xa	1635	ST2497	17/06/2000	6.5	Strike slip	34	0.3856	94.69	54.38	11.503
ulsA-9	Lazio Abruzzo	369xa	175	ST109	07/05/1984	5.9	Normal	44	0.3512	22.74	12.99	12.630
ulsA-10	Pasinler	7089xa	2290	ST557	10/07/2001	5.4	Strike slip	32	0.1916	84.07	14.53	23.147
ulsA-11	Montenegro (aftershock)	234ya	108	ST68	24/05/1979	6.2	Thrust	30	0.7541	24.56	13.70	5.882
ulsA-12	South Iceland	6269ya	1635	ST2497	17/06/2000	6.5	Strike slip	34	0.4192	94.69	24.60	10.579
ulsA-13	Campano Lucano	290ya	146	ST96	23/11/1980	6.9	Normal	32	3.1662	71.93	19.12	1.401
ulsA-14	Campano Lucano	290xa	146	ST96	23/11/1980	6.9	Normal	32	2.1206	60.24	10.75	2.092

M_w magnitude; R_{ep} epicentral distance; *PGA* Peak Ground Acceleration; *DUR* Total duration; $\mathbf{D_{Tr}}$ Trifunac duration; *S.F.* Scale Factor

Table 5 Details of selected ground motions for Lamezia site, SLS limit state, soil type C

Label	Earthquake name	Wave ID	EQ ID	Station ID	Date	M_w	Fault Mech	R_{ep} [km]	PGA [m/s^2]	DUR [s]	D_{Tr} [s]	S.F. [-]
slsC-1	Northridge	458xa	99	ST_24087	17/01/1994	6.7	Reverse	11	3.3738	39.98	23.93	0.758
slsC-2	Northridge	458ya	99	ST_24087	17/01/1994	6.7	Reverse	11	3.0210	39.98	19.78	0.846
slsC-3	Erzincan	465xa	78	ERZ	13/03/1992	6.6	Strike-slip	9	4.8594	20.78	11.76	0.526
slsC-4	Friuli 4th shock	428ya	75	BUI	15/09/1976	5.9	Reverse	11	0.7949	25.89	13.39	3.216
slsC-5	EMILIA (Pianura Padana)	313xa	133	SAN0	29/05/2012	6	Reverse	5	1.7116	32.05	6.19	1.494
slsC-6	N Miyagi Prefecture	34xa	15	MYG010	25/07/2003	6.1	Reverse	10	1.9513	78.89	17.33	1.310
slsC-7	Izmit (aftershock)	111xa	40	YPT	31/08/1999	5.1	Normal	14	0.1355	42.13	27.94	18.861
slsC-8	Adana	1726ya	561	ST549	27/06/1998	6.3	Strike slip	30	2.6442	29.18	20.13	0.967
slsC-9	Spitak	439ya	213	ST173	07/12/1988	6.7	Thrust	36	1.7958	22.98	11.12	1.423
slsC-10	Izmit (aftershock)	6963xa	473	ST3268	13/09/1999	5.8	Oblique	38	0.3975	120.28	61.51	6.431
slsC-11	Adana	1726xa	561	ST549	27/06/1998	6.3	Strike slip	30	2.1575	29.20	17.77	1.185
slsC-12	Calabria	168ya	80	ST44	11/03/1978	5.2	Normal	33	0.3354	19.23	14.25	7.622
slsC-13	Filippias	1908xa	229	ST126	16/06/1990	5.5	Thrust	44	0.1937	23.89	20.96	13.196
slsC-14	Izmit	1230xa	472	ST576	17/08/1999	7.6	Strike slip	39	0.8976	53.04	31.38	2.848

M_w magnitude; R_{ep} epicentral distance; *PGA* Peak Ground Acceleration; *DUR* Total duration; $\mathbf{D_{Tr}}$ Trifunac duration; *S.F.* Scale Factor

Table 6 Details of selected ground motions for Lamezia site, ULS limit state, soil type

Label	Earthquake name	Wave ID	EQ ID	Station ID	Date	M_w	Fault Mech	R_{ep} [km]	PGA [m/s^2]	DUR [s]	D_{Tr} [s]	S.F. [-]
ulsC-1	Erzincan	465xa	78	ERZ	13/03/1992	6.6	Strike-slip	9	4.8594	20.78	11.76	0.870
ulsC-2	Duzce	466xa	39	AI_011_DZC	12/11/1999	7.1	Strike-slip	5	5.1469	145.91	10.65	1.549
ulsC-3	EMILIA (Pianura Padana)	312ya	133	MRN	29/05/2012	6	reverse	4	2.8899	35.30	3.39	2.060
ulsC-4	EMILIA (Pianura Padana)	313ya	133	SAN0	29/05/2012	6	reverse	5	2.1736	32.05	4.46	4.900
ulsC-5	Christchurch	391ya	149	SMTC	13/06/2011	6	reverse	15	0.9137	75.04	20.23	3.329
ulsC-6	Yamaguchi Prefecture	88ya	28	YMG003	25/06/1997	5.8	Strike-slip	10	1.3449	27.26	3.41	2.327
ulsC-7	Christchurch	340ya	142	PPHS	21/02/2011	6.2	reverse	14	1.9239	38.31	16.05	44.804
ulsC-8	Izmit (aftershock)	6414ya	473	ST3127	13/09/1999	5.8	Oblique	91	0.0999	111.96	63.79	1.693
ulsC-9	Adana	1726ya	561	ST549	27/06/1998	6.3	Strike slip	30	2.6442	29.18	20.13	4.706
ulsC-10	Manjil	479xa	230	ST188	20/06/1990	7.4	Oblique	81	0.9513	52.19	36.44	3.998
ulsC-11	Izmit	4343ya	472	ST2574	17/08/1999	7.6	Strike slip	96	1.1197	129.24	42.77	1.474
ulsC-12	Izmit	1226xa	472	ST553	17/08/1999	7.6	Strike slip	100	3.0377	27.17	14.05	3.456
ulsC-13	Manjil	475xa	230	ST184	20/06/1990	7.4	Oblique	91	1.2953	29.49	17.87	4.517
ulsC-14	Izmit	1251ya	472	ST773	17/08/1999	7.6	Strike slip	92	0.9911	138.52	59.94	0.870

M_w magnitude; R_{ep} epicentral distance; *PGA* Peak Ground Acceleration; *DUR* Total duration; $\mathbf{D_{Tr}}$ Trifunac duration; *S.F.* Scale Factor

Table 7 Design parameters of equivalent SDOF braced RC frames

Case ID		μ_F^* (–)	μ_D^* (–)	$d_{targ,ULS}^*$ (mm)	$F_{y,D}^*$ (kN)	$T_{eff,F+D}^*$ (s)	$\xi_{eq,F+D}^*$ (%)
3 storey, ULS, soil A	rc3-sA-μ_F^*1-μ_D^*4	1.0	4.0	19.0	75.0	0.31	11.9
	rc3-sA-μ_F^*1-μ_D^*8	1.0	8.0	19.0	66.0	0.31	12.3
	rc3-sA-μ_F^*1-μ_D^*12	1.0	12.0	19.0	65.0	0.30	12.5
	rc3-sA-μ_F^*max-μ_D^*4	1.3	4.0	24.4	30.0	0.40	16.0
	rc3-sA-μ_F^*max-μ_D^*8	1.3	8.0	24.4	28.0	0.40	16.4
	rc3-sA-μ_F^*max-μ_D^*12	1.3	12.0	24.4	28.0	0.40	16.5
3 storey, ULS, soil C	rc3-sC-μ_F^*1-μ_D^*4	1.0	4.0	19.0	76.0	0.30	12.0
	rc3-sC-μ_F^*1-μ_D^*8	1.0	8.0	19.0	67.0	0.30	12.4
	rc3-sC-μ_F^*1-μ_D^*12	1.0	12.0	19.0	66.0	0.30	12.6
	rc3-sC-μ_F^*max-μ_D^*4	1.3	4.0	24.4	35.0	0.40	16.3
	rc3-sC-μ_F^*max-μ_D^*8	1.3	8.0	24.4	32.0	0.40	16.7
	rc3-sC-μ_F^*max-μ_D^*12	1.3	12.0	24.4	30.0	0.40	16.7
6 storey, ULS, soil A	rc6-sA-μ_F^*1-μ_D^*4	1.0	4.0	37.5	210.0	0.52	16.8
	rc6-sA-μ_F^*1-μ_D^*8	1.0	8.0	37.5	190.0	0.53	17.9
	rc6-sA-μ_F^*1-μ_D^*12	1.0	12.0	37.5	180.0	0.54	18.1
	rc6-sA-μ_F^*max-μ_D^*4	1.3	4.0	48.8	95.0	0.68	17.1
	rc6-sA-μ_F^*max-μ_D^*8	1.3	8.0	48.8	85.0	0.69	17.7
	rc6-sA-μ_F^*max-μ_D^*12	1.3	12.0	48.8	80.0	0.69	17.7
6 storey, ULS, soil C	rc6-sC-μ_F^*1-μ_D^*4	1.0	4.0	37.5	280.0	0.49	19.0
	rc6-sC-μ_F^*1-μ_D^*8	1.0	8.0	37.5	260.0	0.49	20.6
	rc6-sC-μ_F^*1-μ_D^*12	1.0	12.0	37.5	250.0	0.50	21.0
	rc6-sC-μ_F^*max-μ_D^*4	1.5	4.0	56.3	220.0	0.63	22.7
	rc6-sC-μ_F^*max-μ_D^*8	1.5	8.0	56.3	190.0	0.65	23.7
	rc6-sC-μ_F^*max-μ_D^*12	1.5	12.0	56.3	180.0	0.66	24.0
9 storey, ULS, soil A	rc9-sA-μ_F^*1-μ_D^*4	1.0	4.0	47.7	230.0	0.63	15.3
	rc9-sA-μ_F^*1-μ_D^*8	1.0	8.0	47.7	200.0	0.60	15.9
	rc9-sA-μ_F^*1-μ_D^*12	1.0	12.0	47.7	190.0	0.60	16.1
	rc9-sA-μ_F^*max-μ_D^*4	1.2	4.0	57.2	130.0	0.80	15.4
	rc9-sA-μ_F^*max-μ_D^*8	1.2	8.0	57.2	115.0	0.80	15.9
	rc9-sA-μ_F^*max-μ_D^*12	1.2	12.0	57.2	110.0	0.80	16.0
9 storey, ULS, soil C	rc9-sC-μ_F^*1-μ_D^*4	1.0	4.0	47.7	400.0	0.50	19.4
	rc9-sC-μ_F^*1-μ_D^*8	1.0	8.0	47.7	375.0	0.60	21.2
	rc9-sC-μ_F^*1-μ_D^*12	1.0	12.0	47.7	370.0	0.60	21.9
	rc9-sC-μ_F^*max-μ_D^*4	1.6	4.0	76.3	190.0	0.80	20.5
	rc9-sC-μ_F^*max-μ_D^*8	1.6	8.0	76.3	170.0	0.80	21.3
	rc9-sC-μ_F^*max-μ_D^*12	1.6	12.0	76.3	160.0	0.80	21.4

Table 8 Design parameters of equivalent SDOF braced steel frames

Case ID		μ_F^* (-)	μ_D^* (-)	$d_{targ,ULS}^*$ (mm)	$F_{y,D}^*$ (kN)	$T_{eff,F+D}^*$ (s)	$\xi_{eq,F+D}^*$ (%)
2 storey, ULS, soil A	st2-sA-μ_F^*1-μ_D^*4	1.0	4.0	110.4	35.0	1.00	6.1
	st2-sA-μ_F^*1-μ_D^*8	1.0	8.0	110.4	31.0	1.00	6.1
	st2-sA-μ_F^*1-μ_D^*12	1.0	12.0	110.4	29.0	1.01	6.1
	st2-sA-μ_F^*max-μ_D^*4	n.a	n.a	n.a	n.a	n.a	n.a
	st2-sA-μ_F^*max-μ_D^*8	n.a	n.a	n.a	n.a	n.a	n.a
	st2-sA-μ_F^*max-μ_D^*12	n.a	n.a	n.a	n.a	n.a	n.a
2 storey, ULS, soil C	st2-sC-μ_F^*1-μ_D^*4	1.0	4.0	110.4	210.0	0.90	10.6
	st2-sC-μ_F^*1-μ_D^*8	1.0	8.0	110.4	190.0	0.90	11.0
	st2-sC-μ_F^*1-μ_D^*12	1.0	12.0	110.4	180.0	0.90	11.0
	st2-sC-μ_F^*max-μ_D^*4	1.1	4.0	121.4	130.0	1.00	10.7
	st2-sC-μ_F^*max-μ_D^*8	1.1	8.0	121.4	120.0	1.00	11.0
	st2-sC-μ_F^*max-μ_D^*12	1.1	12.0	121.4	115.0	1.00	11.0
4 storey, ULS, soil A	st4-sA-μ_F^*1-μ_D^*4	1.0	4.0	186.5	77.0	1.86	7.7
	st4-sA-μ_F^*1-μ_D^*8	1.0	8.0	186.5	71.0	1.90	8.0
	st4-sA-μ_F^*1-μ_D^*12	1.0	12.0	186.5	68.0	1.90	8.0
	st4-sA-μ_F^*max-μ_D^*4	1.1	4.0	195.8	47.0	2.00	7.9
	st4-sA-μ_F^*max-μ_D^*8	1.1	8.0	195.8	41.0	2.00	8.0
	st4-sA-μ_F^*max-μ_D^*12	1.1	12.0	195.8	39.0	2.00	8.0
4 storey, ULS, soil C	st4-sC-μ_F^*1-μ_D^*4	1.0	4.0	186.5	280.0	1.60	12.4
	st4-sC-μ_F^*1-μ_D^*8	1.0	8.0	186.5	250.0	1.60	13.0
	st4-sC-μ_F^*1-μ_D^*12	1.0	12.0	186.5	240.0	1.60	13.1
	st4-sC-μ_F^*max-μ_D^*4	1.3	4.0	242.5	75.0	2.10	13.1
	st4-sC-μ_F^*max-μ_D^*8	1.3	8.0	242.5	67.0	2.10	13.3
	st4-sC-μ_F^*max-μ_D^*12	1.3	12.0	242.5	64.0	2.10	13.4
8 storey, ULS, soil A	st8-sA-μ_F^*1-μ_D^*4	1.0	4.0	275.0	185.0	3.34	12.5
	st8-sA-μ_F^*1-μ_D^*8	1.0	8.0	275.0	160.0	3.43	13.0
	st8-sA-μ_F^*1-μ_D^*12	1.0	12.0	275.0	150.0	3.46	13.0
	st8-sA-μ_F^*max-μ_D^*4	1.1	4.0	300.0	85.0	3.90	11.1
	st8-sA-μ_F^*max -μ_D^*8	1.1	8.0	300.7	70.0	3.97	11.3
	st8-sA-μ_F^*max-μ_D^*12	1.1	12.0	300.0	65.0	3.99	11.2
8 storey, ULS, soil C	st8-sC-μ_F^*1-μ_D^*4	1.0	4.0	275.0	460.0	2.69	17.0
	st8-sC-μ_F^*1-μ_D^*8	1.0	8.0	275.0	410.0	2.78	18.3
	st8-sC-μ_F^*1-μ_D^*12	1.0	12.0	275.0	390.0	2.82	18.7
	st8-sC-μ_F^*max-μ_D^*4	1.3	4.0	355.4	200.0	3.74	16.6
	st8-sC-μ_F^*max-μ_D^*8	1.3	8.0	355.4	150.0	3.94	16.8
	st8-sC-μ_F^*max-μ_D^*12	1.3	12.0	355.4	125.0	4.05	16.4

Table 9 Characteristics of "rc3" MDOF bare frame (F)

Storey level	$m_{(i)}$(ton)	$\phi_{1(i)}$ [a] (-)	$k_{el,F(i)}$(kN/mm)	$F_{y,F(i)}$(kN)
1	27.2	0.32	46.5	255.7
2	27.2	0.75	28.8	213.1
3	14.9	1.00	25.1	127.9

[a]normalized mode shape components

Table 10 Characteristics of "st8" MDOF bare frame (F)

Storey level	$m_{(i)}$(ton)	$\phi_{1(i)}$ [a] (-)	$k_{el,F(i)}$(kN/mm)	$F_{y,F(i)}$(kN)
1	102.9	0.12	9.6	321.1
2	102.9	0.30	6.4	312.2
3	102.9	0.47	6.1	294.3
4	102.9	0.63	6.3	267.6
5	102.9	0.77	6.1	231.9
6	102.9	0.88	7.0	208.2
7	102.9	0.96	8.3	170.7
8	95.7	1.00	15.0	165.2

[a]normalized mode shape components

Funding Open access funding provided by Politecnico di Milano within the CRUI-CARE Agreement. This work was funded by the Italian Department of Civil Protection (DPC) in the frame of the national Research Project DPC-ReLUIS 2019–2021 Work Package WP 15 "*Contributi normativi a isolamento e dissipazione*".

Declarations

Conflict of interest The authors declare that they have no known competing financial interests or personal relationships that could have appeared to influence the work reported in this paper.

Open Access This article is licensed under a Creative Commons Attribution 4.0 International License, which permits use, sharing, adaptation, distribution and reproduction in any medium or format, as long as you give appropriate credit to the original author(s) and the source, provide a link to the Creative Commons licence, and indicate if changes were made. The images or other third party material in this article are included in the article's Creative Commons licence, unless indicated otherwise in a credit line to the material. If material is not included in the article's Creative Commons licence and your intended use is not permitted by statutory regulation or exceeds the permitted use, you will need to obtain permission directly from the copyright holder. To view a copy of this licence, visit http://creativecommons.org/licenses/by/4.0/.

References

Akcelyan S, Lignos DG, Hikino T, Nakashima M (2016) Evaluation of simplified and state-of-the-art analysis procedures for steel frame buildings equipped with supplemental damping devices based on E-defense full-scale shake table tests. J Struct Eng 142(6):04016024

Ambraseys N, Smit P, Sigbjornsson R, Suhadolc P, Margaris B (2002) Internet-Site for European strong-motion data. European Commission, Research-Directorate General, Environment and Climate Programme.

ANSI, AISC (2016) AISC 360–16, Specification for structural steel buildings. American Institute of steel construction, Chicago

Applied Technology Council, ATC-40 (1996) Seismic evaluation and retrofit of concrete buildings, California.
ASCE/SEI Standard 41–17. Seismic evaluation and retrofit of existing buildings. American Society of Civil Engineers, Reston, Virginia, USA; 2017.
Baird A, Smith T, Palermo A, Pampanin, S (2014) Experimental and numerical study of U-shape flexural plate (UFP) dissipators. In New Zealand Society for Earthquake Engineering Conference; University of Canterbury: Christchurch, New Zealand.
Baker JW (2007) Quantitative classification of near-fault ground motions using wavelet analysis. Bull Seismol Soc Am 97(5):1486–2150
Barbagallo F, Bosco M, Marino EM, Rossi PP, Stramondo P (2017) A multi-performance deisgn method for seismic upgrading of existing RC frames by BRBs. Earthquake Eng Struct Dynam 46:1099–1119. https://doi.org/10.1002/eqe
Bergami AV, Nuti C (2013) A design procedure of dissipative braces for seismic upgrading structures. Earthq Struct 4(1):85–108
Buchanan A, Iqbal A, Palermo AG, Pampanin S (2007) Improved seismic performance of LVL post-tensioned walls coupled with UFP devices. In Proceedings of the 8th Pacific Conference on Earthquake Engineering, Singapore, 5–7 December, pp. 1–9.
Casarotti C, Monteiro R, Pinho R (2009) Verification of spectral reduction factors for seismic assessment of bridges. BNZSEE(NZSEE Bulletin) 42(2):111–121
CEN 2003. Eurocode 3: design of steel structures: Part 1–1: general rules and rules for buildings. European Committee for Standardization, Bruxelles, Belgium.
CEN 2004. Eurocode 8: design of structures for earthquake resistance—Part 1: general rules, seismic actions and rules for buildings, EN1998-1:2004. European Committee for Standardization, Bruxelles, Belgium.
CEN 2005. Eurocode 8: design of structures for earthquake resistance—Part 2: bridges, EN1998-2:2005+A1:2011. European Committee for Standardization, Bruxelles, Belgium.
CEN 2009. EN 15129 European Standard, anti-seismic devices. european committee for standardization: Brussels, Belgium.
Christopolous C, Filiatrault A (2006) Principles of passive supplemental damping and seismic isolation. IUSS Press, Pavia
CSi (2017). Analysis reference manual for SAP2000®. SAP2000 version 21, Integrated solution for structural analysis and design. Computers and Structures, Inc., Berkeley, California, USA.
CSLLPP—Consiglio Superiore dei Lavori Pubblici (2018). Norme Tecniche per le Costruzioni - NTC2018. Gazzetta Ufficiale della Repubblica Italiana, No. 42 of 20 February 2018. Rome, Italy, (in Italian)
De Domenico D, Ricciardi G, Takewaki I (2019) Design strategies of viscous dampers for seismic protection of building structures: a review. Soil Dyn Earthq Eng 118:144–165
De Domenico D, Ricciardi G (2019) Earthquake protection of structures with nonlinear viscous dampers optimized through an energy-based stochastic approach. Eng Struct 179:523–539
De Domenico D, Tubaldi E, Takewaki I, Karavasilis T, DallAsta A, Lavan O (2020) Recent advances and applications of seismic isolation and energy dissipation devices. Front Built Environ. https://doi.org/10.3389/fbuil.2020.00126
Del Gobbo GM, Williams MS, Blakeborough A (2018) Comparing fluid viscous damper placement methods considering total-building seismic performance. Earth Eng Struct Dyn 47(14):2864–2886
Di Cesare A, Ponzo FC, Nigro D (2014) Assessment of the performance of hysteretic energy dissipation bracing systems. Bull Earthq Eng 12(6):2777–2796. https://doi.org/10.1007/s10518-014-9623-z
Di Cesare A, Ponzo FC (2017) Seismic retrofit of reinforced concrete frame buildings with hysteretic bracing systems: design procedure and behaviour factor. Hindawi Shock Vib. https://doi.org/10.1155/2017/2639361
Di Cesare A, Ponzo FC, Nigro D, Pampanin S, Smith T (2017) Shaking table testing of post-tensioned timber frame building with passive energy dissipation systems. Bull Earthq Eng 2017(15):4475–4498
Di Cesare A, Ponzo FC, Lamarucciola N, Nigro D (2020) Dynamic seismic response of nonlinear displacement dependent devices versus testing required by codes experimental case studies. Appl Sci. https://doi.org/10.3390/app10248857
Durucan C, Dicleli M (2010) Analytical study on seismic retroftting of reinforced concrete buildings using steel braces with shear link. Eng Struct 32:2995–3010
Dwairi HM, Kowalsky MJ, Nau JM (2007) Equivalent damping in support of direct displacement-based design. J Earthq Eng 11(4):512–530
Faleschini F, Zanini MA, Toska K (2019) Seismic reliability assessment of code-conforming reinforced concrete buildings made with electric arc furnace slag aggregates. Eng Struct 195:324–339

Foti D, Ruggiero F, Sabbà MF, Lerna MA (2020) Dissipating frames for seismic retrofitting and building energy-efficiency. Infrastructures 5:74
Gandelli E, Taras A, Distl J, Quaglini V (2019) Seismic retrofit of hospitals by means of hysteretic braces: influence on acceleration-sensitive non-structural components. Front Built Environ Earthq Eng 5:100
Granello G, Palermo A, Pampanin S, Pei S, van de Lindt J (2020) Pres-Lam buildings: state-of-the-art. J Struct Eng 146:04020085
Gullu A, Smyrou E, Khajehdehi A et al (2019) Numerical modelling of energy dissipative steel cushions. Int J Steel Struct 19:1331–1341
Guo G, Yang D (2018) Duration effect of near-fault pulse-like ground motions and identification of most suitable duration measure. Bull Earth Eng 16:5095–5119
Iervolino I, Galasso C (2010) E. REXEL: computer aided record selection for code-based seismic structural analysis. Bull Earthq Eng 8:339–362
Jacobsen LS (1930) Steady forced vibrations as influenced by damping. ASME Transactione 52(1):169–181
Javanmardi A, Ibrahim Z, Ghaedi K, Ghadim HB, Hanif MU (2020) State-of-the-art review of metallic dampers: testing, development and implementation. Arch Comp Methods Eng 27:455–478
Kammouh O, Silvestri S, Palermo M, Cimellaro GP (2018) Performance-based seismic design of multistory frame structures equipped with crescent-shaped brace. Struct Control Health Monit 25:2079
Karavasilis TL (2016) Assessment of capacity design of columns in steel moment resisting frames with viscous dampers. Soil Dyn Earth Eng 88:215–222
Kelly JM, Skinner RI, Heine AJ (1972) Mechanisms of energy absorption in special devices for use in earthquake resistant structures. BNZSEE 5(3):53–68
Mazza F, Vulcano A (2015) Displacement-based design procedure of damped braces for the seismic retrofitting of RC framed buildings. Bull Earthq Eng 13:2121–2143. https://doi.org/10.1007/s10518-014-9709-7
Mazza F, Mazza M, Vulcano A (2015) Displacement-based seismic design of hysteretic damped braces for retrofitting in-elevation irregular RC framed buildings. Soil Dyn Earthq Eng 69:115–124. https://doi.org/10.1016/j.soildyn.2014.10.029
Mazza F (2016a) Nonlinear seismic analysis of r.c. framed buildings with setbacks retrofitted by damped braces. Eng Struct 126:559–570. https://doi.org/10.1016/j.engstruct.2016.07.055
Mazza F (2016b) Nonlinear seismic analysis of unsymmetric-plan structures retrofitted by hysteretic damped braces. Bull Earthq Eng 14:1311–1331. https://doi.org/10.1007/s10518-016-9873-z
Mazza F, Mazza M (2019) Seismic retrofitting of gravity-loads designed r.c. framed buildings combining CFRP and hysteretic damped braces. Bull Earthq Eng 17:3423–3445. https://doi.org/10.1007/s10518-019-00593-5
McKenna, F., Fenves, G.L. Scott, M.H. (2000). Open system for earthquake engineering simulation. PEER Report, Berkeley, CA.
Mohammadi RK, Garoosi MR, Hajirasouliha I (2019) Practical method for optimal rehabilitation of steel frame buildings using buckling restrained brace dampers. Soil Dyn Earthq Eng 123:242–251
Mohsenian V, Mortezaei A (2018) New energy absorbing system for seismic retrofitting of frame structures with slender braces. Bull Earthq Eng 17:2715–2739
Montuori R, Nastri E, Piluso V (2015) Advances in theory of plastic mechanism control: closed form solution for MR-Frames. Earthq Eng Struct Dyn 44:1035–1054
Morillas L, Escolano-Margarit D (2020) Estimation of cyclic demand in metallic yielding dampers installed on frame structures. Appl Sci 10:4364
Muto K (1969): Earthquake resistant design of 36-storied Kasumigaseki Building. 4th World Conference on Earthquake Engineering, Santiago, Chile.
Nabid N, Hajirasouliha I, Petkovski M (2018) Performance-based optimisation of RC frames with friction wall dampers using a low-cost optimisation method. Bull Earthq Eng 16(10):5017–5040
Nuzzo I, Losanno D, Caterino N (2019) Seismic design and retrofit of frames structures with hysteretic dampers: a simplified displacement-based procedure. Bull Earthq Eng 17:2787–2819. https://doi.org/10.1007/s10518-019-00558-8
Nuzzo I, Ciliento F, Caterino N (2020) DIBRAST: A computer-aided seismic design procedure for frame structures equipped with hysteretic devices. Front Built Environ 6:13
O'Reilly GJ, Sullivan TJ (2016) Direct displacement-based seismic design of eccentrically braced steel frames. J Earthquake Eng 20(2):243–278. https://doi.org/10.1080/13632469.2015.1061465
Ozkaynak H, Khajehdehi A, Gullu A et al (2018) Uni-axial behavior of energy dissipative steel cushions. Steel Compos Struct 27(6):661–674
Palermo M, Pieraccini L, Dib A, Silvestri S, Trombetti T (2017) Experimental tests on Crescent Shaped Braces hysteretic devices. Eng Struct 144:185–200

Palermo M, Ricci I, Gagliardi S, Silvestri S, Trombetti T, Gasparini G (2014) Multi-performance seismic design through an enhanced first-storey isolation system. Eng Struct 59:495–506

Palermo M, Silvestri S, Gasparini G, Trombetti T (2015) Crescent shaped braces for the seismic design of building structures. Mater Struct 48:1485–1502

Ponzo, F.C., Di Cesare, A., Arleo, G., Totaro P. (2010). Protezione sismica di edifici esistenti con controventi dissipativi di tipo isteretico: aspetti progettuali ed esecutivi. Progettazione Sismica 4: 50–75 (in Italian)

Ponzo FC, Di Cesare A, Lamarucciola N, Nigro D (2019) Seismic design and testing of post-tensioned timber buildings with dissipative bracing systems. Front Built Environ 5:104

Priestley MJN, Calvi GM, Kowalsky MJ (2007) Displacement-based seismic design of structures – 2nd edition. Eucentre, ISBN: 88–85701–05–2.

Quintana Gallo P, Carradine DM, Bazaez R (2020) State of the art and practice of seismic-resistant hybrid timber structures. Eur J Wood Prod, 1–24.

Skinner RI, Kelly JM, Heine AJ (1974) Hysteretic dampers for earthquake-resistant structures. Earthquake Eng Struct Dynam 3(3):287–296

Trifunac MD, Brady AG (1975) A study on the duration of strong earthquake ground motion. Bull Seismol Soc Am 65(3):581–626

Vayas I, Vamvatsikos D, Thanopoulos P (2017) I. 11.00: Innovative systems for seismic resistance: The INNOSEIS Project. ce/papers, 1(2–3), 3375–3384.

Watanabe A, Hitomi Y, Saeki E, Wada A, Fujimoto M (1988) Properties of brace encased in buckling-restraining concrete and steel tube. In Proceedings of the Ninth World Conference on Earthquake Engineering, Tokyo, Japan, 2–9 August, Volume 4, pp. 719–724.

Publisher's Note Springer Nature remains neutral with regard to jurisdictional claims in published maps and institutional affiliations.